NACA

RESEARCH MEMORANDUM

INVESTIGATION OF THRUST AND DRAG CHARACTERISTICS

OF A PLUG-TYPE EXHAUST NOZZLE

By Donald P. Hearth and Gerald C. Gorton

Lewis Flight Propulsion Laboratory
Cleveland, Ohio

CLASSIFIED DOCUMENT

This material contains information affecting the National Defense of the United States within the meaning of the espionage laws, Title 18, U.S.C., Secs. 793 and 794, the transmission or revelation of which in any manner to an unauthorized person is prohibited by law.

NATIONAL ADVISORY COMMITTEE
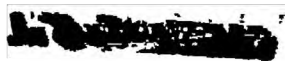# FOR AERONAUTICS
WASHINGTON
February 19, 1954

CONFIDENTIAL

NATIONAL ADVISORY COMMITTEE FOR AERONAUTICS

RESEARCH MEMORANDUM

INVESTIGATION OF THRUST AND DRAG CHARACTERISTICS

OF A PLUG-TYPE EXHAUST NOZZLE

. By Donald P. Hearth and Gerald C. Gorton

SUMMARY

An investigation was conducted in the 8- by 6-foot supersonic wind tunnel on the external and internal characteristics of a plug-type exhaust nozzle. Two positions of the center plug, one simulating a convergent nozzle and the other a convergent-divergent nozzle, were investigated. Data were obtained at free-stream Mach numbers of 0.1, 0.6, 1.6, and 2.0 over a pressure-ratio range of 1 to 20 and angles of attack of zero and 8°.

Results of this investigation indicated that the plug nozzle had thrust-minus-drag performance over the entire pressure-ratio range comparable with equivalent conventional nozzles. The effect of the exhaust jet on the external aerodynamics was similar to results observed for conventional nozzles. In addition, the thrust characteristics were generally insensitive to external flow and good agreement was noted with data obtained on comparable plug nozzles in quiescent air.

INTRODUCTION

Supersonic jet-engine operation requires that the exhaust nozzle for such engines be operated over a range of pressure ratios. Moreover, for a turbojet engine equipped with afterburner, for example, throat-area variation may also be desired. Numerous forms of variable-geometry nozzles have been proposed for jet-engine application, and preliminary evaluation of several practical designs has been made in quiescent air (refs. 1 to 4).

One of the more promising variable-geometry nozzles is the plug type (refs. 3 to 5), which utilizes axial translation of a streamlined centerbody to achieve a variation both in the minimum area and in the expansion ratio. Although the plug nozzle does not offer an independent variation of these two quantities, it may be designed to satisfy a desired throat-area variation with expansion-ratio change. If not

designed to satisfy conditions over an entire schedule, a plug nozzle
may at least have applications as a two-position device such as for
afterburner off and on operation.

In order to fully evaluate exhaust nozzles, the effect of external
flow on the internal nozzle thrust characteristics, as well as the effect
of the jet on external aerodynamics, is required. A comprehensive
program has therefore been undertaken in the NACA Lewis 8- by 6-foot
supersonic wind tunnel. Investigated as a part of this program was a
plug-type exhaust nozzle installed on a generalized NACA jet-exit model.
Two positions of the center plug simulating the two end points of a
throat-area - expansion ratio schedule were investigated. In one posi-
tion the nozzle was physically a convergent-divergent nozzle, while in the
other position the nozzle was physically a convergent nozzle. Thrust
and drag characteristics are presented for free-stream Mach numbers of
0.1, 0.6, 1.6, and 2.0 at zero angle of attack over a pressure-ratio
range from 1 to 20. Some internal data are also presented at angles of
attack of 8°. All data were obtained with a jet temperature of 400° F.

APPARATUS AND PROCEDURE

Installation

The generalized exit model on which the plug nozzle was investigated
is shown installed in the 8- by 6-foot supersonic wind tunnel in figures
1 and 2. The model was supported by two 11-percent-thick horizontal
struts of circular-arc cross section. These struts were attached to
trunnions mounted in the tunnel wall and were rotated to vary the model
angle of attack.

The source of the model internal air flow was a separately con-
trolled air supply. Air flow was measured with a sharp-edge orifice,
and the internal model pressure was varied with a butterfly valve
located downstream of the orifice (fig. 1). In order to avoid the
possibility of condensation shocks in the nozzle, the air was preheated
to a temperature of 400° F by means of a conventional turbojet can
combustor. Air was introduced into the model through the hollow support
struts as indicated in figure 1.

Basic Exit Model and Data Reduction

The basic model, shown schematically in figure 3, consisted of
three main components: an outer shell, the "capsule," and an inner
liner. The axially symmetric nose section of the outer shell was of
parabolic contour based on the following equation (x is the axial
distance from the nose tip and y the distance from the model axis):

3138

CH-1 back

$$y = 4\frac{1}{8}\left[1 - \left(\frac{40 - x}{40}\right)^2\right]$$

The parabolic contour extended to a body diameter of $8\frac{1}{4}$ inches at a point 40 inches from the nose. This diameter was maintained for the next 31.60 inches, and a suitable afterbody for the nozzle was added beyond the cylindrical section.

As can be seen from figure 3, the two support struts, through which air was brought into the model, were rigidly attached to the capsule. A turn of 90° was required for the air to flow axially through the model. Since the internal air flow was confined to the capsule and inner liner (maximum internal diameter of 7.0 in.), the external forces were applied only on the outer shell while the internal forces were applied on the capsule and inner liner.

A strain-gage balance located in the nose ahead of the capsule was used to obtain force measurements. In order to separate the internal and external forces, two runs, each with a different balance connection (figs. 3(a) and (b)), were required. The "drag" connection (fig. 3(a)) was such that only the forces on the outer shell were applied to the balance, and total external drag could then be obtained. The "thrust-minus-drag" connection (fig. 3(b)) was such that both the inner liner and the outer shell were restrained by the balance; thus, the sum of the external and the internal forces on these surfaces was measured. The internal forces were equivalent to the change in internal axial momentum from the inner-liner entrance (station 2) to the nozzle exit (station 4). Since calibration indicated that the air entering the capsule had no component in the axial direction, the momentum at station 2 was assumed equal to the net internal axial force acting on the capsule. The thrust-minus-drag connection, therefore, yielded the jet thrust minus the total external drag of the model. The details of utilizing the balance readings (symbols defined in appendix A) in obtaining these forces are discussed in appendix B. Adding the external drag force to the measured thrust-minus-drag force yielded the jet thrust of the nozzle. This measured jet thrust was compared with an ideal jet thrust defined as the product of the actual mass flow and the exit velocity corresponding to complete isentropic expansion (see appendix B). The nozzle mass-flow coefficient is defined as the ratio of actual to ideal mass flow passed through the nozzle and was calculated as shown in appendix B. Air flow and preheater fuel flow were measured with an A.S.M.E. orifice and a rotameter, respectively. Additional data obtained included static pressures on the plug, boattail, and base. The instrumentation was located on the top and bottom and also on one side of the plug and boattail as shown in figure 4.

Plug-Nozzle Configuration

The exhaust-nozzle configuration investigated consisted of an internally located plug supported by four struts within a parabolic-shaped boattail. Coordinates of the plug, obtained from the lemniscate of Bernoulli's equation modified for a fineness ratio of 3.0, are presented in table I. Also included in the table are the inner-liner coordinates. The external afterbody, which was connected to the cylindrical section of the basic model at station 71.60, was cylindrical for 3.85 inches and terminated with a parabolic-shaped boattail, the equation for which is indicated in figure 4.

The two plug positions investigated are shown in figure 4 (see fig. 5 for the variation in flow areas). The convergent-divergent position was such that the end of the plug coincided with the end of the afterbody at station 83.75. This configuration corresponded to a convergent-divergent nozzle with a design pressure ratio of 5.8 and a throat area of 0.140 square foot. The other position of the plug was such that the throat area of 0.090 square foot occurred at the end of the afterbody. With the plug in the latter position, the nozzle was physically convergent except for the protruding section of the plug. These two plug positions were designed to simulate the two end points of a variable-throat-area nozzle which, for example, would be required with an afterburner-temperature-ratio variation from 1.0 to 2.4.

RESULTS AND DISCUSSION

External Characteristics

The effect of the jet issuing from the plug nozzle on the boattail pressure distribution is presented in figure 6. Although data are presented only at a free-stream Mach number of 2.0, the trends noted were also obtained at the other Mach numbers investigated. The variation in pressure coefficient $C_{p,a}$ is presented as a function of nozzle pressure ratio such that a negative value of pressure coefficient indicates a drag force while a positive value represents a thrust force. As can be seen from figure 6(a), when the plug was in the convergent-divergent position, the boattail pressures were affected only slightly by the nozzle pressure ratio. However, with the plug in the convergent position (fig. 6(b)), a considerably greater influence of the jet pressure ratio on the boattail pressures was noted (pressures were influenced upstream as much as 0.6 of the jet diameter). These same trends have been noted for conventional nozzles (ref. 6) and are caused by the degree of nozzle underexpansion, especially noticeable with convergent nozzles. Because of the off-design operation of the nozzle, however, a large loss in thrust occurs concurrent with this drag reduction for conventional nozzle types.

3138

Presented in figure 7 is the variation of the boattail pressure-drag coefficient $C_{D,a}$ (based on maximum cross-sectional area of the body) with the nozzle pressure ratio for free-stream Mach numbers of 2.0, 1.6, and 0.6. Data are presented for both plug positions and were obtained from integration of boattail pressure distributions such as shown in figure 6.

As expected from the pressure distributions, the boattail pressure drag with the plug in the convergent-divergent position (fig. 7(a)) was virtually unaffected by nozzle pressure ratio even at pressure ratios in excess of the design value of 5.8. Included on the figure for comparison purposes is the boattail pressure-drag variation at a Mach number of 2.0 of a conventional convergent-divergent nozzle. For the conventional nozzle the boattail drag decreased at pressure ratios above the design value (5.3). This difference in trends may be due in part to the difference in flow angles (both internal and external) in the plane at which the boattail terminates. If two nozzles are to be considered for the same engine operating point, the throat areas would have to be the same. Since the throat areas for the two nozzles shown on figure 7(a) were different, a comparison of absolute values of boattail drag is not made.

With the plug in the convergent position, the boattail pressure drag (fig. 7(b)) was reduced by the jet issuing from the nozzle for pressure ratios in excess of 4 to 5 supersonically and for all pressure ratios with subsonic external flow. Included in this figure is the boattail drag variation at a Mach number of 2.0 for a conventional convergent nozzle. As shown for comparable Mach numbers, the drag reduction for the conventional nozzle occurred at lower values of nozzle pressure ratio than for the plug nozzle shown. In addition to a difference in the flow angles, it should be pointed out that part of the expansion of the flow from the throat of the plug nozzle occurred toward the center of the jet, thereby tending to reduce the growth of the jet. Since both the conventional convergent and the convergent plug nozzles had the same throat areas, a comparison of the absolute values of boattail pressure drag is permissible. Because of the area occupied by the plug itself, the projected afterbody area was less than that required by a conventional convergent nozzle. As expected, therefore, the values of boattail pressure drag were appreciably lower for the plug nozzle.

The nature of the jet influence on the boattail aerodynamics is apparent from the schlieren photographs presented in figure 8. (It should be noted that the dark horizontal strip near the center of the jet is the upper half of the wake from the horizontal support struts.) Photographs at low and high pressure ratios for a Mach number of 2.0 are presented for the convergent-divergent plug position (figs. 8(a) and (b)) and for the convergent plug position (figs. 8(c) and (d)). A large change in nozzle pressure ratio caused very little movement of the

trailing shock with the plug in the convergent-divergent position but a
large movement of the trailing shock with the plug in the convergent
plug position. This trailing shock (ref. 6) was caused by the inter-
action of the jet and the external stream and appears near the body as
a series of compression waves due to thickening of the body boundary
layer. The movement of this shock was primarily responsible for the
change in the boattail pressure distributions and drag variations pre-
sented in figures 6 and 7. However, it should be noted that the trail-
ing shock moved only about half the distance upstream, as did the
observed pressure feedback through the boundary layer (fig. 6).

In order to maintain free relative movement between the inner liner
and the outer shell, a clearance between these components was allowed.
This clearance resulted in an appreciable base area. Influence of the
jet on base pressure is indicated by the variations of base pressure
coefficient $C_{p,b}$ and is presented in figure 9. For comparison purposes,
base pressure coefficients of conventional nozzles are included on this
figure. At comparable Mach numbers, although the general trend is the
same, the jet did not increase the base pressure coefficient of the
convergent-divergent plug-nozzle configuration as much as for a conven-
tional convergent-divergent nozzle (fig. 9(a)). However, with the plug
in the convergent position (fig. 9(b)) the effect of the jet on the base
pressure coefficient was similar to that observed for a conventional
convergent nozzle. It should be noted that the difference in flow angles
and the jet expansion effect discussed previously in this section are
factors influencing these curves.

Presented in figure 10 is the variation of the total external drag
coefficient for both plug positions at free-stream Mach numbers of 0.6,
1.6, and 2.0. It is felt that, although the absolute value of the total
external drag is not significant because of interference from the support
struts, the trend with pressure ratio is significant. Because of instru-
mentation failure for this particular investigation, external-drag
values from the strain-gage balance could not be obtained from the drag
connection as anticipated. The total external drag was, however, obtained
by adding the measured boattail pressure drag and the measured base drag
to the sum of the nose pressure plus the friction drag. The sum of these
latter forces was obtained from an unpublished investigation which
utilized the same basic model as well as the same over-all body length.
The sharp decrease in total drag of the convergent plug position with
increasing nozzle pressure ratio as compared with the total drag of the
convergent-divergent position is the cumulative effect of pressure
ratio on boattail and base drags.

3138

3138

Internal Characteristics

Nozzle mass-flow coefficients (see appendix B) are presented in figure 11 for the convergent plug position at free-stream Mach numbers of 2.0, 1.6, 0.6, and 0.1 and angles of attack of zero and 8°. Although the amount of data was limited and the scatter pronounced, it appears that there was very little effect of nozzle pressure ratio, free-stream Mach number, and angle of attack. Moreover, the average value of flow coefficient, which was 0.988, was equivalent to that of a well-designed conventional nozzle. Values of flow coefficient were not obtained with the plug in the convergent-divergent position. However, flow coefficients of the same order of magnitude as for the convergent plug position might be anticipated.

The internal thrust characteristics, obtained from force measurements, are presented in figure 12 as the ratio of measured thrust to ideal thrust (see appendix B) for a range of free-stream Mach numbers and for angles of attack of zero and 8°. The variation of thrust ratio with nozzle pressure ratio for the convergent-divergent position of the plug is presented in figure 12(a). Within the data scatter, there appeared to have been very little effect of either free-stream Mach number or angle of attack on jet thrust. Contrary to expectations, the peak jet-thrust ratio, a value of 0.98, did not decrease for pressure ratios above the design value of 5.8 but held essentially constant.

For the convergent plug position (fig. 12(b)), there was generally little if any effect of free-stream Mach number or angle of attack on the jet thrust. The general level of the thrust ratio was low, a peak of 0.935 at P_3/p_0 of 4.0, and was probably caused by negative thrust being exerted on the protruding portion of the plug at the low pressure ratios. Moreover, in contrast with conventional convergent nozzles, only a small decrease in the thrust ratio was observed as the nozzle pressure ratio was increased above 4.0.

Static-pressure distributions on the plug for the convergent-divergent plug position and for the convergent plug position are presented in figures 13 and 14, respectively. Data are presented at zero angle of attack over a range of pressure ratios for all free-stream Mach numbers.

As indicated in figure 13, the flow for the convergent-divergent plug position generally expanded supersonically, and very good agreement was obtained with the isentropic one-dimensional flow theory. When the nozzle became far overexpanded $(P_3/p_0 < 2.8)$, a shock entered the nozzle. For such operation, the internal shock system assumed a structure such that the static pressure at the nozzle exit was very close to ambient.

With the plug in the convergent position, the static-pressure
distributions (fig. 14) indicate that the flow initially expanded very
rapidly from the throat along the extended section of the plug. In fact,
the initial expansion was so rapid that the flow appears to have expanded
below ambient static pressure at all pressure ratios and all free-stream
Mach numbers investigated. Generally, the flow exhibited the character-
istics of expansion in a diverging-nozzle section.

Presented in figure 15 are typical schlieren photographs of the
flow at the nozzle exit for the convergent plug position at three differ-
ent pressure ratios for each of the Mach numbers of 2.0 and 0.6 and at
zero angle of attack. These photographs serve to indicate the type of
shock structure which produced the pressure distributions of figure 14.

Angle-of-attack data at 8° were obtained for the convergent plug
position at Mach numbers of 2.0 and 1.6. Comparison of pressure distri-
butions on the top and bottom of the plug indicated that up to an 8°
angle of attack no asymmetric loads were applied to the plug.

An alternative method of obtaining jet thrust was employed in
obtaining the nozzle thrust values given in figure 16. The change in
jet thrust through the diverging-nozzle section was obtained from an
integration of the static wall pressures in this section, and the result
was added to the computed thrust of a sonic nozzle to obtain the result-
ing jet thrust at the exit. The jet thrust thus obtained neglected any
friction losses in the nozzle. For purposes of comparison, the thrust-
ratio curves obtained from the force measurements are included in this
figure.

Up to a nozzle pressure ratio of 7.0, for the convergent-divergent
plug position (fig. 16(a)), the thrust data obtained from the pressure
distributions were approximately 2 percent above the same data obtained
from force measurements. Above pressure ratios of 7.0, the two sets of
data disagree in trend. The thrust ratio obtained from pressure inte-
gration peaked at the design point and then decreased as the nozzle
became underexpanded. This trend is consistent with conventional
convergent-divergent nozzle performance (ref. 7). On the other hand,
the jet-thrust ratio determined from force measurements remained essen-
tially constant as the nozzle was underexpanded. Generally the two
sets of data agreed within 2 to 3 percent.

Agreement within 1 percent is indicated for the convergent plug
position (fig. 16(b)). Only data above pressure ratios of 5.0 have been
plotted since the instrumentation was found to be inadequate at lower
pressure ratios because of the numerous shocks and the resulting abrupt
pressure changes occurring on the plug below this pressure ratio. The
pressure integration indicated that at low pressure ratios the protruding
plug contributed a drag force. This drag force decreased in magnitude

as the nozzle pressure ratio was increased until the extended section of the plug contributed a thrust force in the high-pressure-ratio range. This variation in force on the protruding plug no doubt caused the thrust-ratio curve to exhibit the flat characteristics shown.

Compared in figure 17(a) are the thrust ratios for three convergent-divergent nozzles. A comparison of the data obtained in the present investigation with data obtained on a similar plug nozzle investigated in quiescent air (ref. 3) indicates excellent agreement. It also appears that the convergent-divergent plug-type nozzle was comparable on a thrust-ratio basis with a conventional-type nozzle (ref. 7) having essentially the same design point.

A comparison of convergent-type nozzles is made in figure 17(b). Good agreement was again obtained between the present investigation and an investigation on a comparable plug-type nozzle in quiescent air (ref. 4). As expected, the thrust ratio for the plug nozzle was below that of a conventional convergent nozzle (ref. 7) in the low-pressure-ratio range and compared more favorably as the pressure ratio was increased.

Jet-Thrust-Minus-Drag Comparison

A comparison is made in figure 18 of the jet-thrust-minus-drag characteristics of the plug nozzle and comparable conventional nozzles. Calculations were made for the basic model used in the present investigation having a nozzle throat area of 0.090 square foot. The performance of the conventional nozzles was estimated from the thrust data of reference 7 and unpublished drag data such as is shown in figures 7 and 9. It should be noted that the inlet momentum for an over-all engine application was not included in figure 18, thus the use of jet thrust rather than net thrust.

The jet-thrust-minus-drag performance of the plug nozzle with the convergent-divergent position (fig. 18(a)) was comparable over the entire range with that of a conventional convergent-divergent nozzle having essentially the same design point. With the plug in the convergent position (fig. 18(b)), the thrust-minus-drag performance of the plug nozzle also compared favorably over the entire range with a conventional convergent nozzle. The low thrust ratios noted for this plug position in the low-pressure-ratio region (fig. 17(b)) were evidently more than compensated for by the smaller amount of boattail drag (fig. 7(b)).

SUMMARY OF RESULTS

The following results were obtained from an investigation conducted in the 8- by 6-foot supersonic wind tunnel on a plug-type exhaust nozzle tested in a convergent and a convergent-divergent position with an expansion ratio of 1.45:

1. The thrust-minus-drag performance of the plug nozzles investigated compared favorably over the entire pressure-ratio range with conventional nozzles having the same design points.

2. Internal performance was generally insensitive to external flow and was essentially the same for the range of free-stream Mach numbers investigated as obtained on comparable plug nozzles investigated in quiescent air.

3. The effect of the exhaust jet on the external aerodynamics was similar to that for conventional nozzles in that the boattail drag and the base pressure were more influenced by the convergent position than by the convergent-divergent position.

4. Nozzle flow coefficients with choked flow of the same order of magnitude as for conventional nozzles were virtually unaffected by pressure ratio and external flow.

5. During angle-of-attack operation, no asymmetric loads were obtained on the plug when extended beyond the afterbody.

Lewis Flight Propulsion Laboratory
    National Advisory Committee for Aeronautics
        Cleveland, Ohio, December 11, 1953

APPENDIX A

SYMBOLS

The following symbols are used in this report:

A	area, sq ft
B_D	strain-gage-balance reading for drag connection, lb
B_{F-D}	strain-gage-balance reading for thrust-minus-drag connection, lb
C_D	drag coefficient, $D/q_0 A_m$
$C_{F,c}$	corrected thrust coefficient, $F_c/q_0 A_m$
C_f	flow coefficient, m/m_i
C_p	pressure coefficient, $(p - p_0)/q_0$
D	drag force, lb
F	jet thrust, $mV_4 + A_4(p_4 - p_0)$, lb
F_c	jet thrust based on throat area of 0.090 sq ft, lb
F_i	ideal jet thrust, $mV_{4,i}$, lb
F/F_i	thrust ratio
f/a	fuel-air ratio
g	acceleration due to gravity, 32.2 ft/sec^2
J	total momentum, $mV + Ap$, lb
M	Mach number
m	mass flow, ρAV, slug/sec
P	total pressure, lb/sq ft
P_3/p_0	nozzle pressure ratio
p	static pressure, lb/sq ft
q	dynamic pressure, $\gamma p M^2/2$, lb/sq ft

R   radius, ft

T   total temperature, $^{\circ}R$

V   velocity, ft/sec

γ ratio of specific heats for air

ρ static density, slug/cu ft

Subscripts:

a   boattail

b   base

i   ideal

m   maximum

t   total

0   free stream

1   before shoulder

2   after shoulder

3   nozzle entrance

4   nozzle exit

*   nozzle throat

3138

3138

APPENDIX B

DATA REDUCTION

External Drag
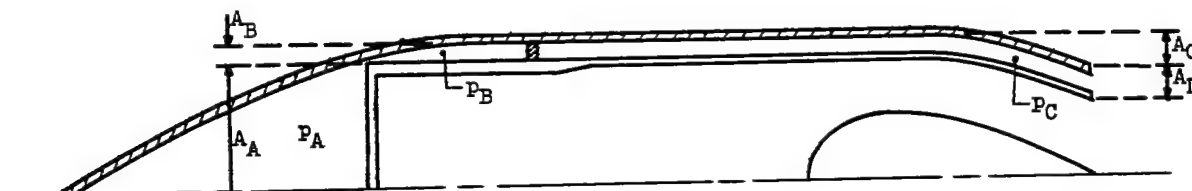
Sketch 1

Total external drag was obtained from the model by use of the drag connection of the strain-gage balance and various pressure measurements. In sketch 1,

$$D_t = B_D + (p_A - p_0)A_A + (p_B - p_0)A_B - (p_C - p_0)A_C - (p_C - p_0)A_D \quad (B1)$$

Measured Jet Thrust
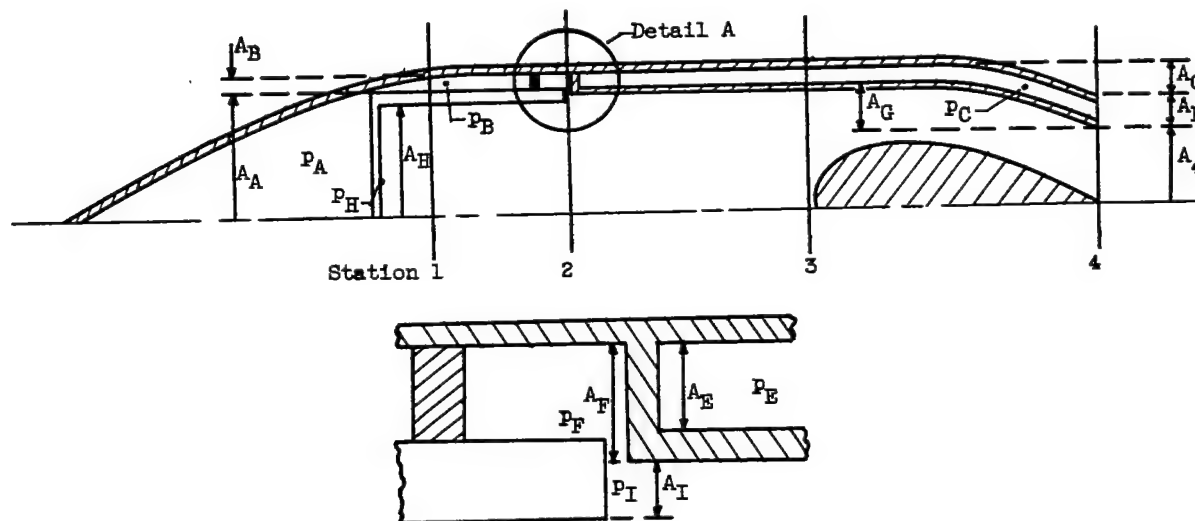
Sketch 2

Jet thrust is defined as

$$F_4 = mV_4 + p_4 A_4 - p_0 A_4 \tag{B2}$$

Equation (B2) is equivalent to

$$F_4 = J_4 - p_0 A_4 \tag{B3}$$

The momentum at station 4 is related to the momentum at station 2 by

$$J_4 = J_2 - \Delta J_{2-3} - \Delta J_{3-4} \tag{B4}$$

Calibration indicated that ΔJ_{2-3} was equal to zero, and since

$$J_2 = p_H A_H + p_I A_I$$

equation (B3) becomes

$$F_4 = p_H A_H + p_I A_I - \Delta J_{3-4} - p_0 A_4 \tag{B5}$$

The change in total momentum between stations 3 and 4 is equal to the absolute force acting on the nozzle (i.e., the inner liner and plug between these two stations). This force plus the total external drag is obtained from the thrust-minus-drag connection of the strain-gage balance:

$$\Delta J_{3-4} + D_t = B_{F-D} + (p_A - p_0)A_A + (p_B - p_0)A_B - (p_C - p_0)A_C -$$

$$(p_C - p_0)A_D + p_C A_G + p_E A_E - p_F A_F \tag{B6}$$

Substitution of ΔJ_{3-4} from equation (B6) into equation (B5) yields the jet thrust minus the total external drag of the model:

$$F_4 - D_t = p_H A_H + p_I A_I - B_{F-D} - (p_A - p_0)A_A - (p_B - p_0)A_B +$$

$$(p_C - p_0)A_C + (p_C - p_0)A_D - p_C A_G - p_E A_E + p_F A_F - p_0 A_4 \tag{B7}$$

The jet thrust can then be calculated by adding a total-external-drag value to the value of jet-thrust-minus-external-drag as obtained from equation (B7).

Ideal Jet Thrust

Ideal jet thrust is defined as the product of the measured mass flow and the ideal exit velocity for complete isentropic expansion.

(A truly ideal nozzle would have the same thrust but with a throat area slightly smaller by the amount of the mass-flow coefficient.) Thus,

$$F_i = mV_{4,i} \qquad \text{(B8)}$$

Equation (B8) is equivalent to

$$F_i = m\left[\left(\frac{2\gamma gRT_1}{\gamma - 1}\right) \frac{\left(\frac{p_3}{p_0}\right)^{\frac{\gamma-1}{\gamma}} - 1}{\left(\frac{p_3}{p_0}\right)^{\frac{\gamma-1}{\gamma}}}\right]^{1/2} \qquad \text{(B9)}$$

The total temperature T_1 of the internal air flow was measured by thermocouples located in the horizontal support struts and was assumed to remain constant throughout the model.

Nozzle Mass-Flow Coefficient

The mass-flow coefficient is defined as the ratio of mass flow actually passed through the nozzle to the amount of mass flow that can ideally be passed through the nozzle. Thus,

$$C_f = \frac{m(1 + f/a)}{p_3 A_* \left(\frac{2}{\gamma + 1}\right)^{\frac{\gamma+1}{2(\gamma-1)}} \sqrt{\frac{\gamma}{gRT_1}}}$$

REFERENCES

1. Lundin, Bruce: Investigation of Several Clamshell Variable-Area Exhaust Nozzles for Turbojet Engines. NACA RM E9B02, 1949.

2. Fleming, William A.: Internal Performance of Several Types of Jet-Exit Configurations for Supersonic Turbojet Aircraft. NACA RM E52K04, 1953.

3. Krull, H. George, Steffen, Fred W., and Ciepluch, Carl C.: Internal Performance Characteristics of Variable-Throat Plug- and Vaned-Type Convergent-Divergent Nozzles. NACA RM E53D09, 1953.

3138

4. Ciepluch, Carl C., Krull, H. George, and Steffen, Fred W.: Prelim-
   inary Investigation of Performance of Variable-Throat Extended-
   Plug-Type Nozzle over Wide Range of Nozzle Pressure Ratios.
   NACA RM E53J28, 1954.

5. Sterbentz, William H., and Wilcox, Fred A.: Investigation of Effects
   of Movable Exhaust-Nozzle Plug on Operational Performance of 20-
   Inch Ram Jet. NACA RM E8D22, 1948.

6. Cortright, Edgar, and Kochendorfer, Fred D.: Jet Effects on Flow
   over Afterbodies in Supersonic Stream. NACA RM E53H25, 1953.

7. Krull, H. George, and Steffen, Fred W.: Performance Characteristics
   of One Convergent and Three Convergent-Divergent Nozzles. NACA
   RM E52H12, 1952.

3138

3138

CH-3

TABLE I. - PRINCIPLE DIMENSIONS OF PLUG NOZZLE

[Minimum flow area for convergent-divergent plug position, 0.140 sq ft;
minimum flow area for convergent plug position, 0.090 sq ft; expan-
sion ratio of convergent-divergent plug position, 1.451; maximum
model cross-sectional area, 0.371 sq ft.]
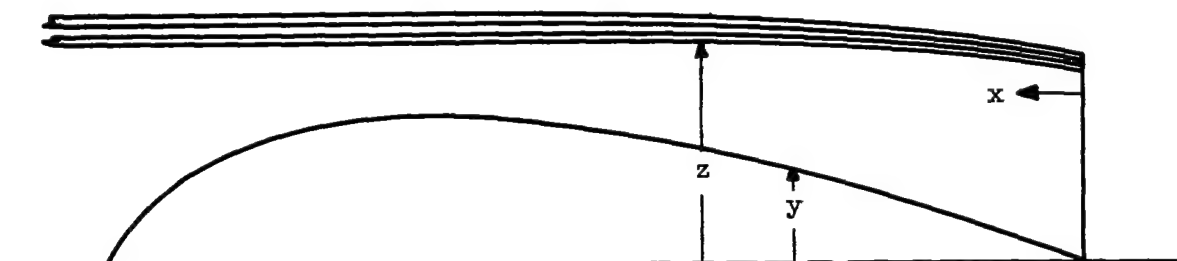
Coordinates of plug and nozzle		
x, in.	y, in.	z, in.
0	0	3.055
1.36	.631	3.170
1.93	.881	3.230
2.39	1.071	3.270
2.78	1.229	3.310
3.13	1.353	3.330
4.60	1.817	3.440
5.78	2.100	3.480
6.89	2.280	3.500
7.90	2.370	3.500
8.84	2.405	3.500
9.68	2.385	3.500
10.50	2.310	3.500
11.20	2.190	3.500
11.83	2.030	3.500
12.42	1.852	3.500
12.93	1.640	3.500
13.38	1.402	3.500
13.73	1.142	3.500
14.02	.872	3.500
14.21	.588	3.500
14.40	0	3.500
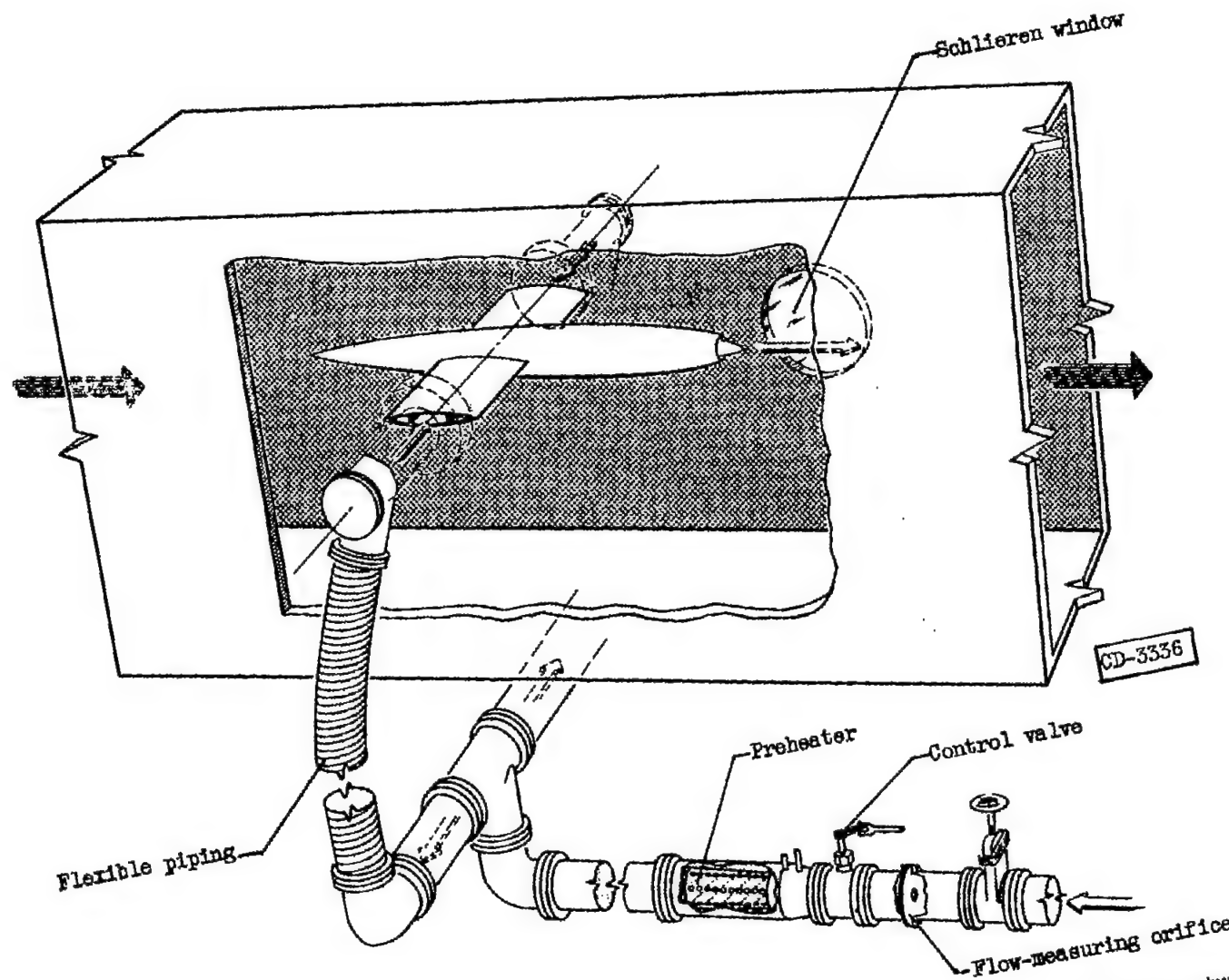
Figure 1. - Schematic drawing of jet-exit model installed in 8- by 6-foot supersonic wind tunnel.

CD-3336

3138
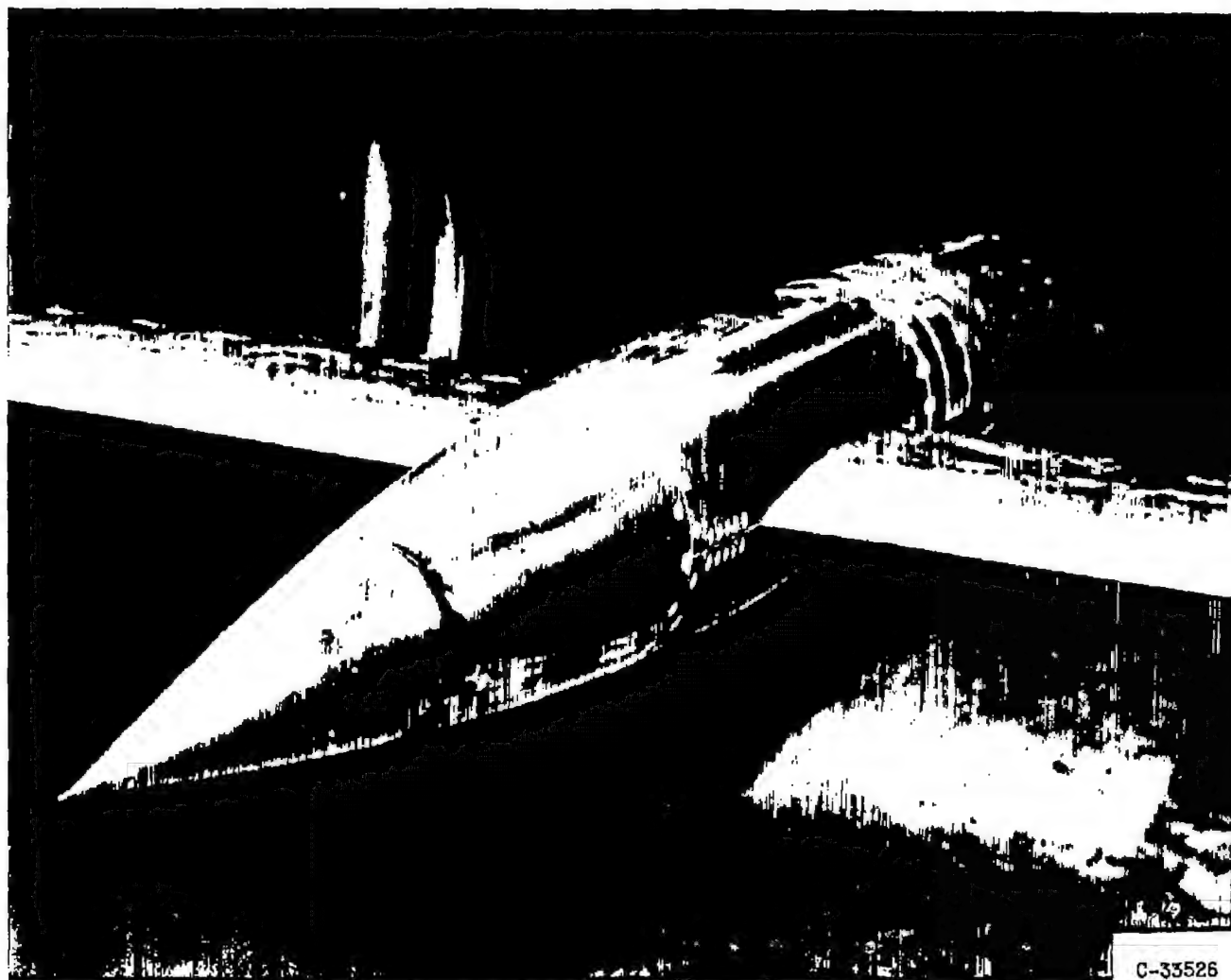
Figure 2. - Photograph of jet-exit model in 8- by 6-foot supersonic wind tunnel.
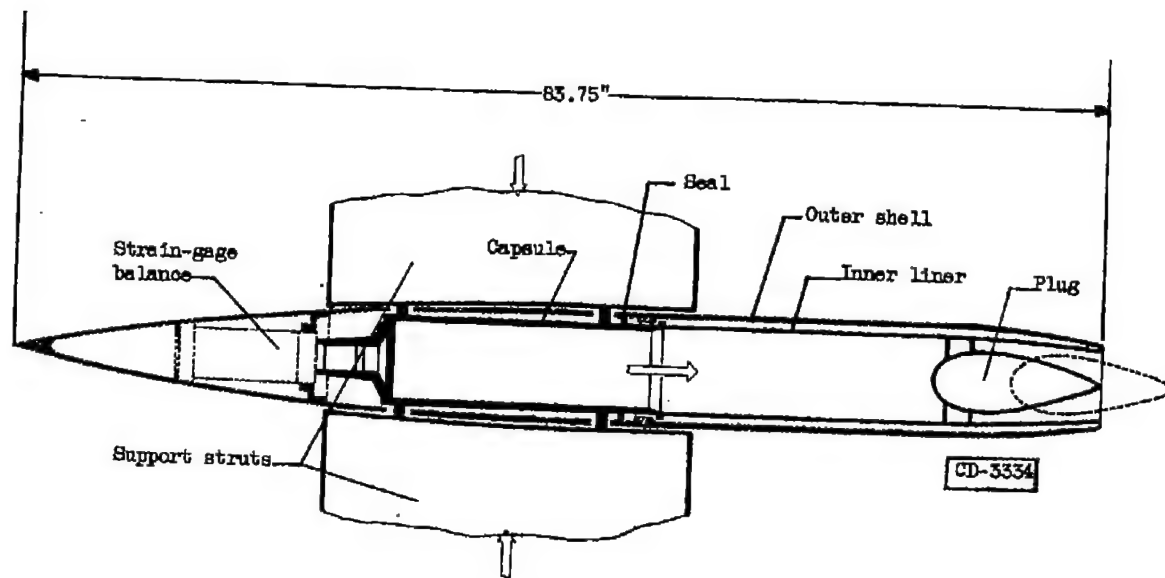
(a) "Drag" connection.
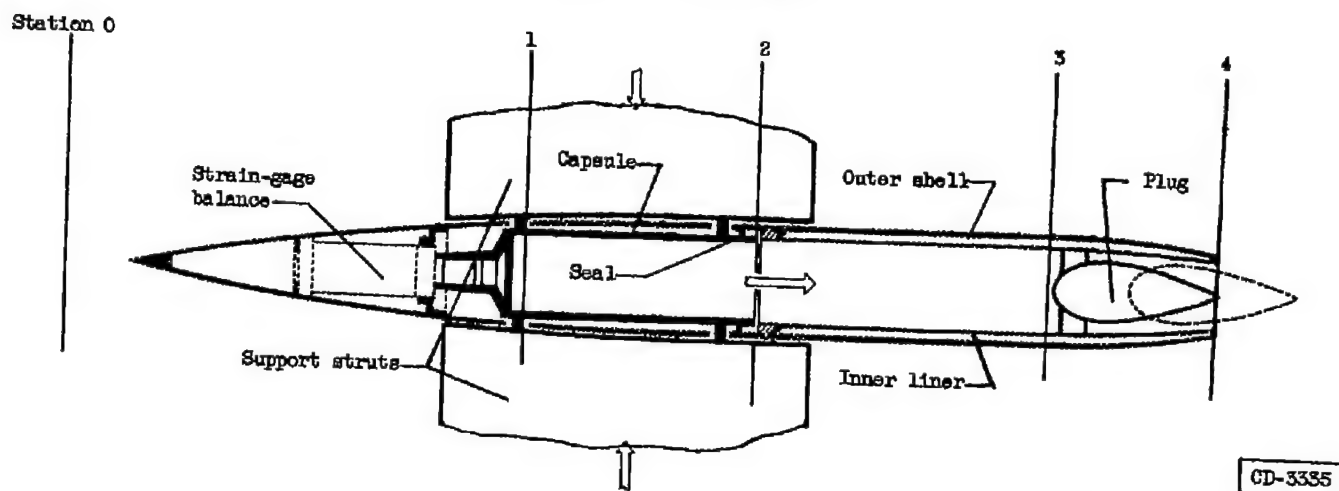
(b) "Thrust-minus-drag" connection.

Figure 3. - Schematic diagram of jet-exit model.

Equation of boattail: $y = 4\frac{1}{8}\left[1 - \left(\frac{z}{18}\right)^2\right]$
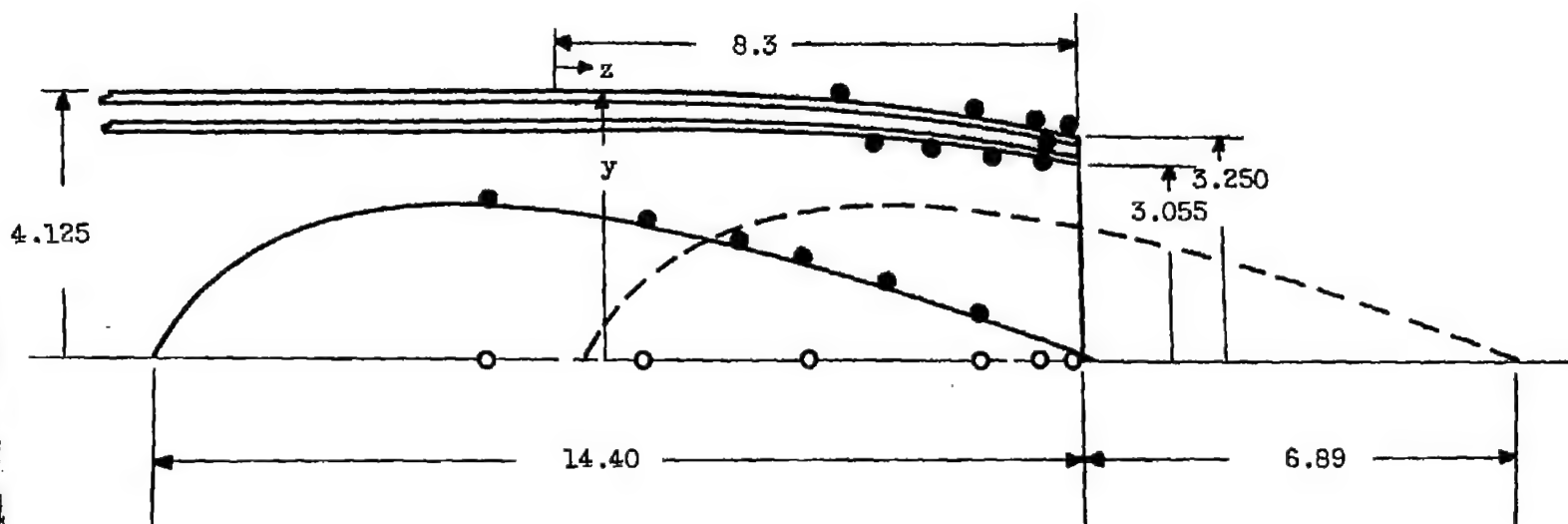
Static-pressure orifice

●   Top and bottom
○   Side

Figure 4. - Schematic drawing of plug-nozzle - afterbody configuration including static-pressure instrumentation. (All dimensions in inches.)
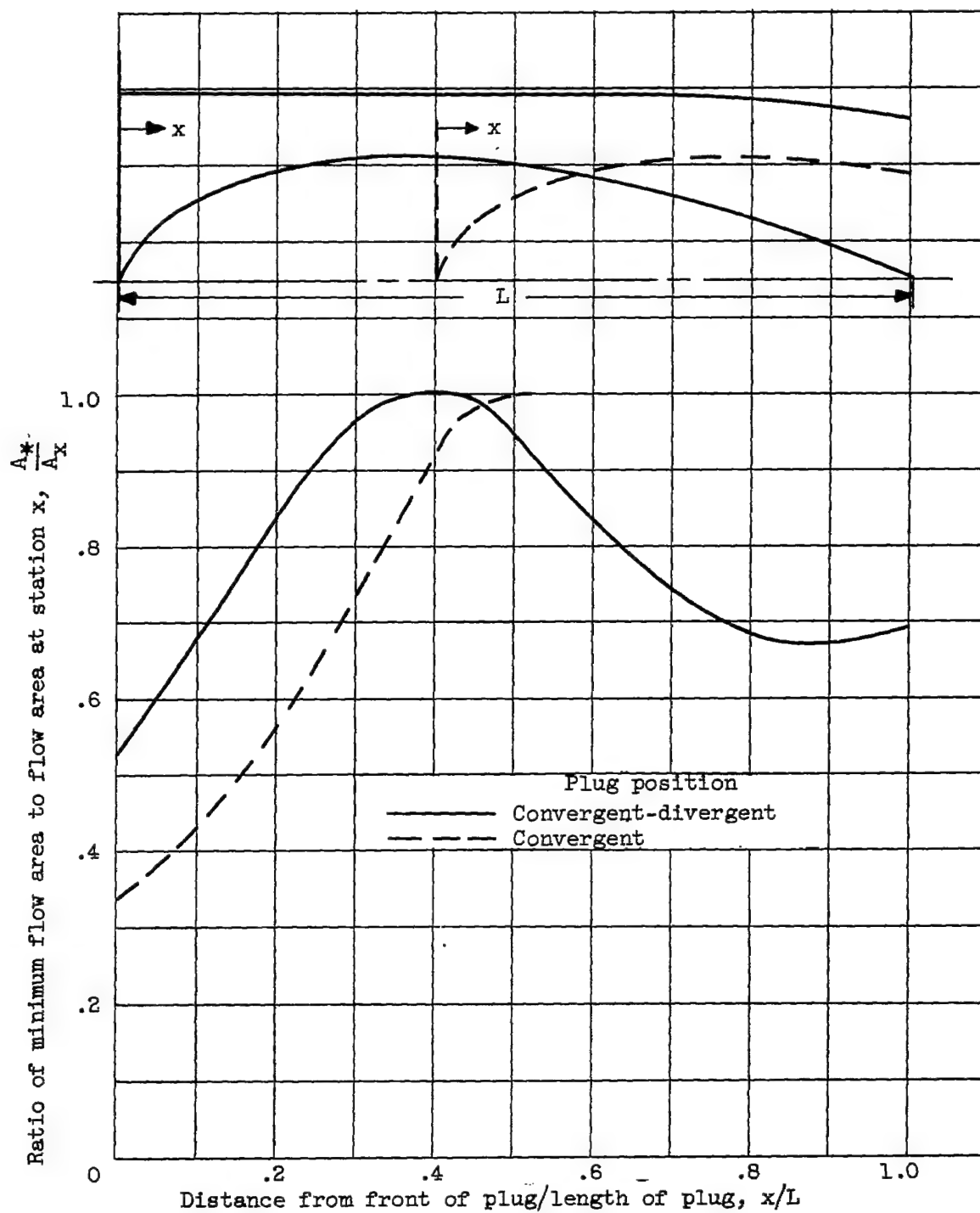
Figure 5. - Flow-area variation for two plug positions investigated.

3138
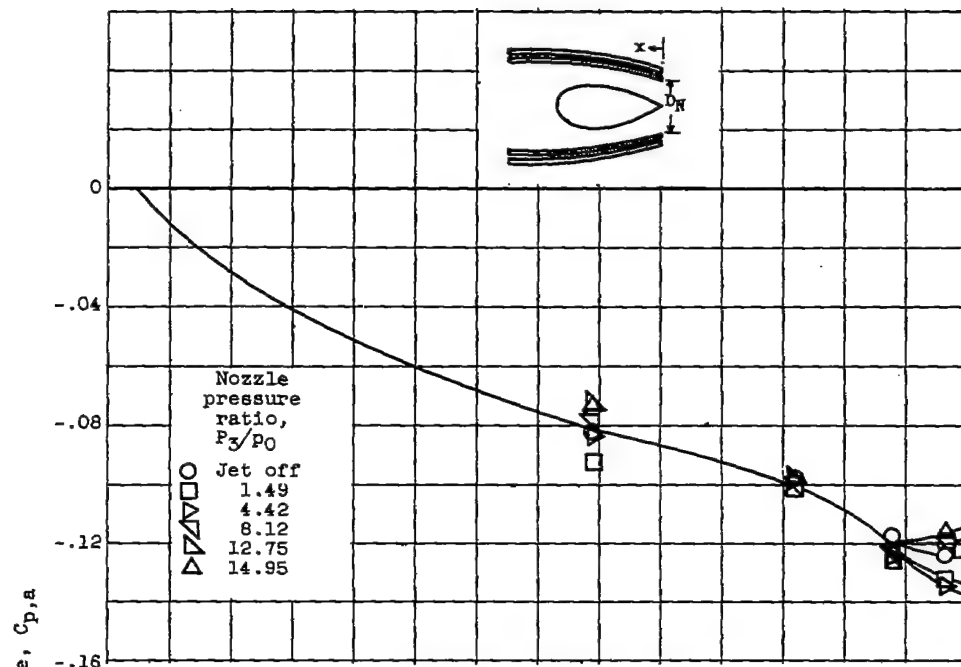
(a) Convergent-divergent plug position.
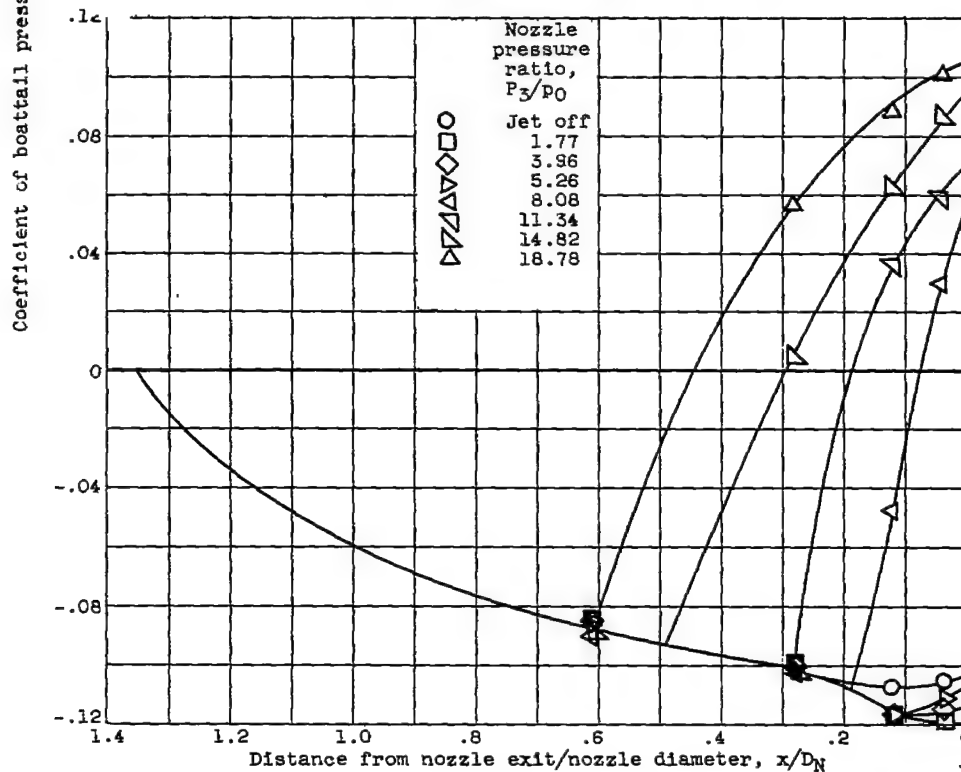
(b) Convergent plug position.

Figure 6. - Boattail pressure distributions at free-stream Mach number of 2.0 and zero angle of attack.

(a) Convergent-divergent plug position.

(b) Convergent plug position.
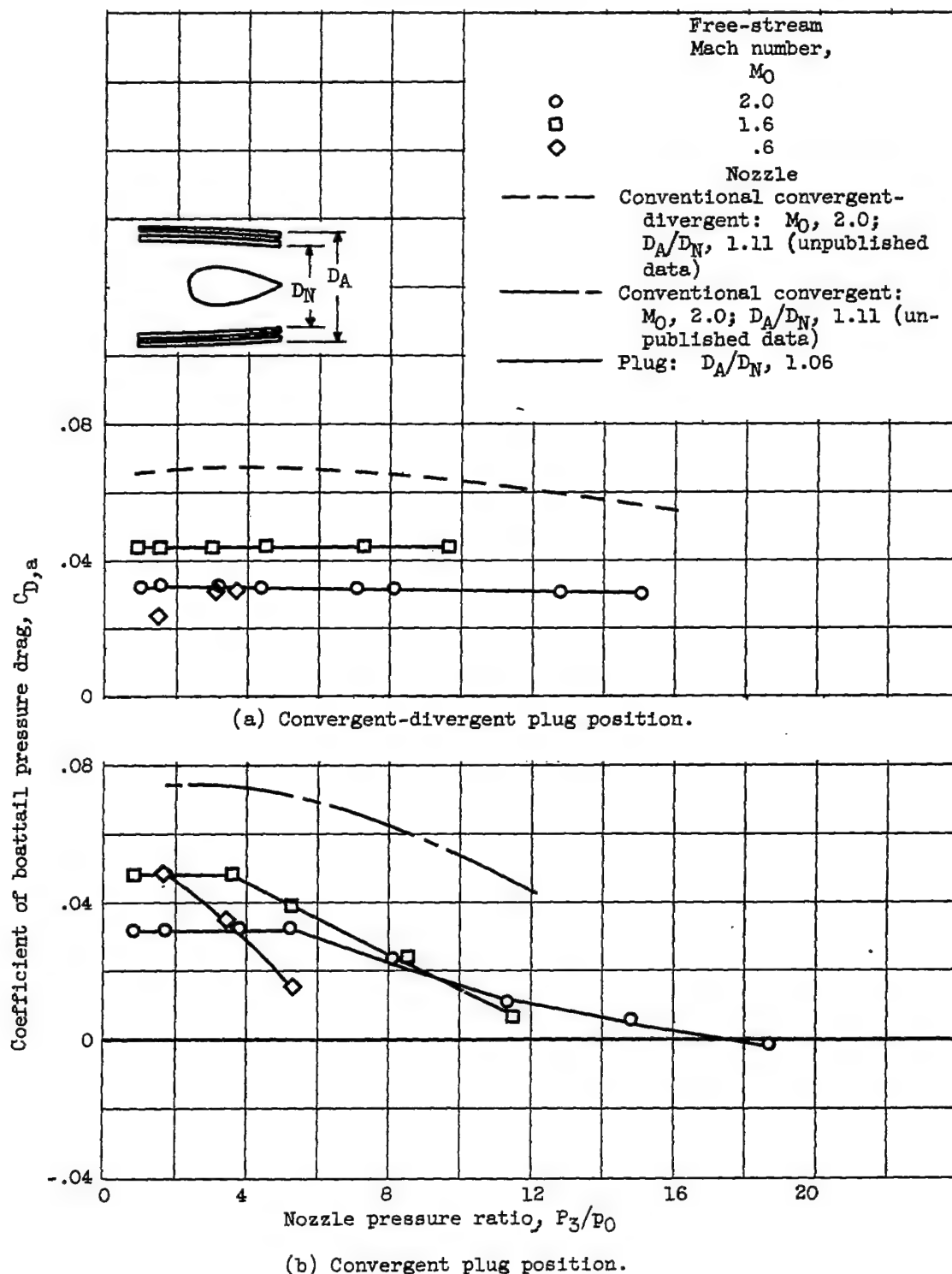
Figure 7. - Variation of boattail pressure-drag coefficient
with nozzle pressure ratio at zero angle of attack.

3138

CH-4
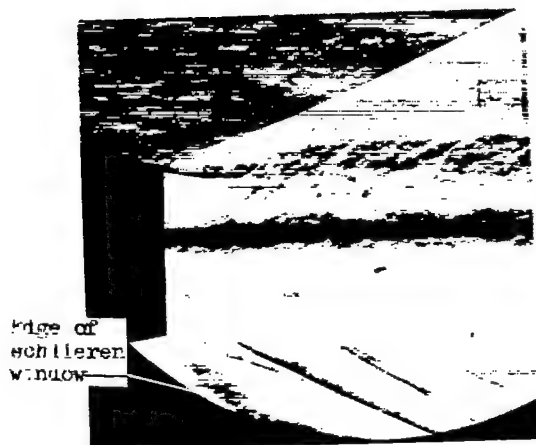
(a) Convergent-divergent plug position. Nozzle pressure ratio, 4.36.
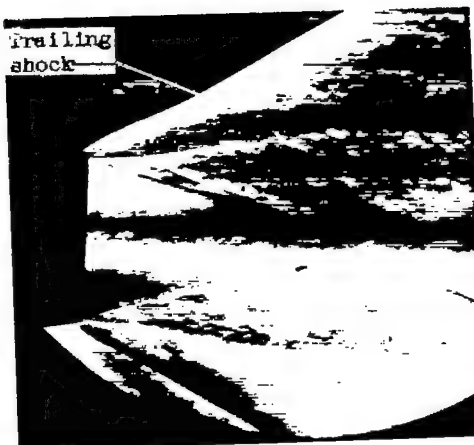
(b) Convergent-divergent plug position. Nozzle pressure ratio, 14.76.
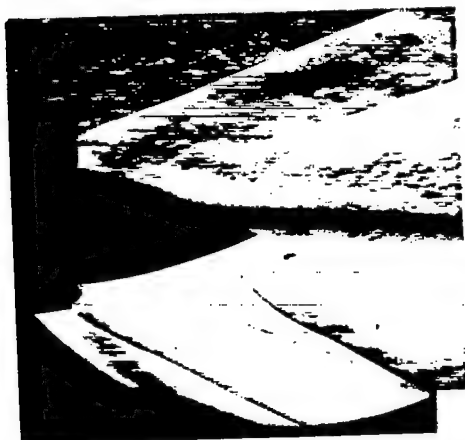
(c) Convergent plug position. Nozzle pressure ratio, 3.51.
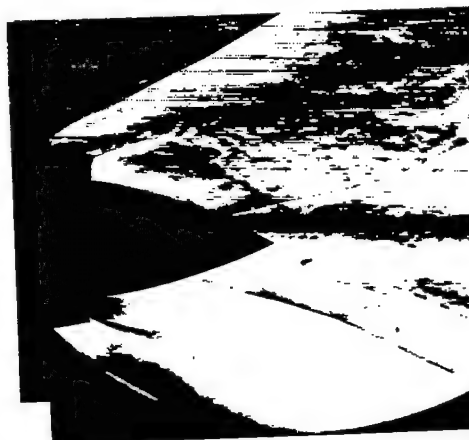
(d) Convergent plug position. Nozzle pressure ratio, 14.26.

C-34392

Figure 8. - Schlieren photographs of external aerodynamics of boattail at free-stream Mach number of 2.0 and zero angle of attack.
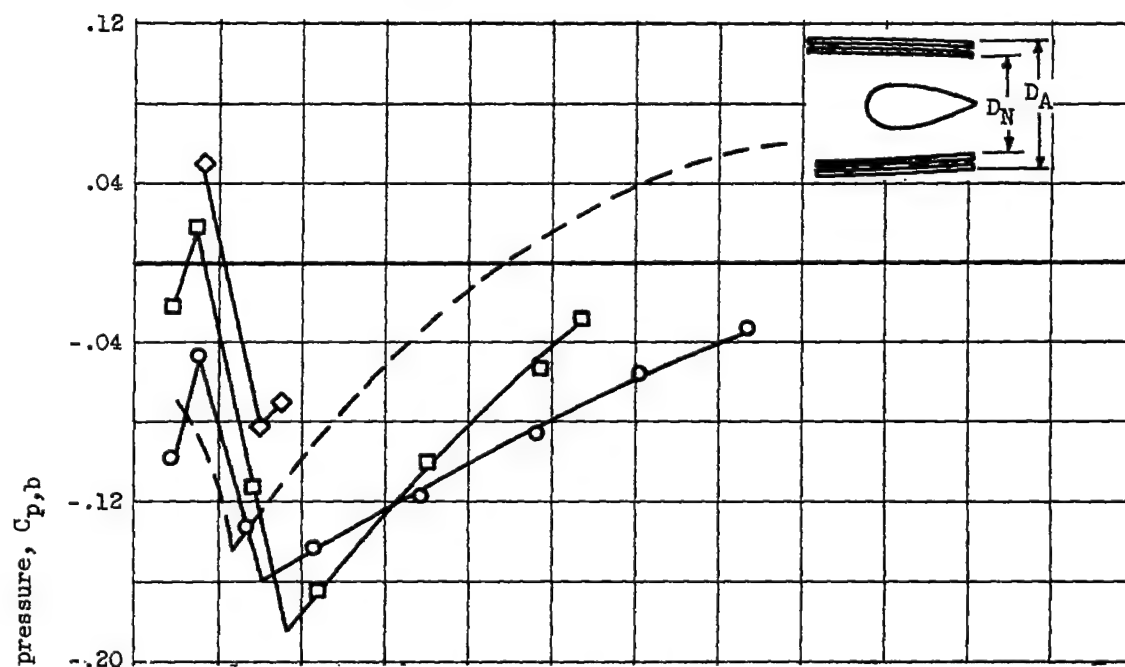
(a) Convergent-divergent plug position.
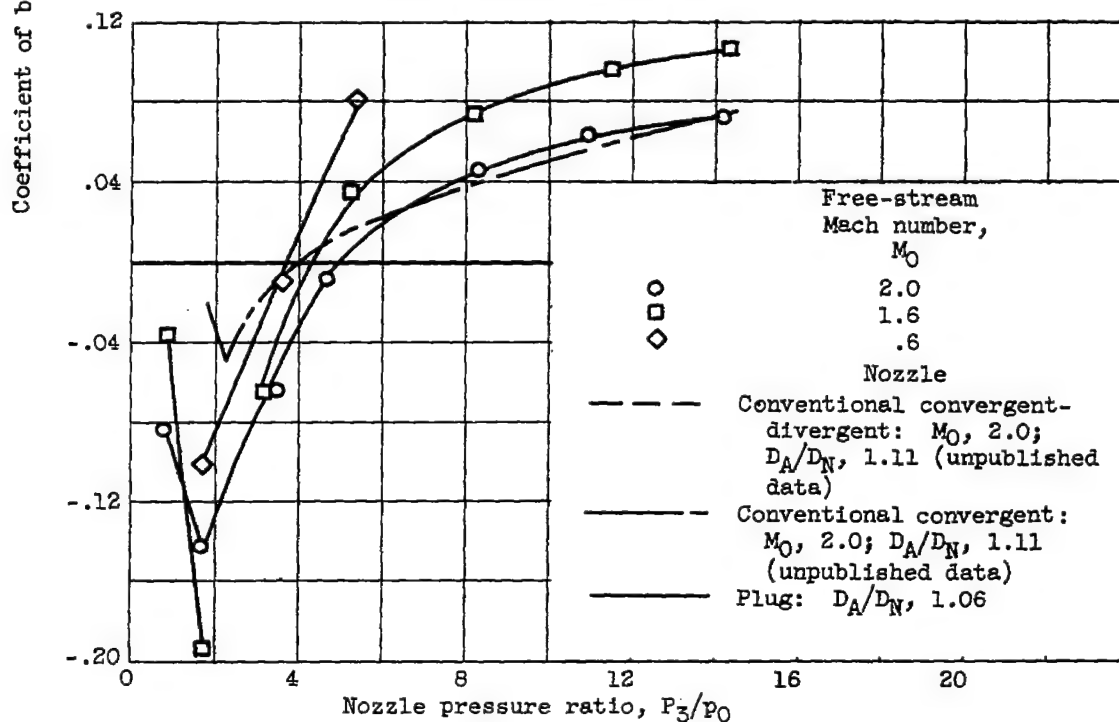
(b) Convergent plug position.

Figure 9. - Variation of base pressure coefficient with nozzle pressure
ratio at zero angle of attack.

3138

CH-4 back
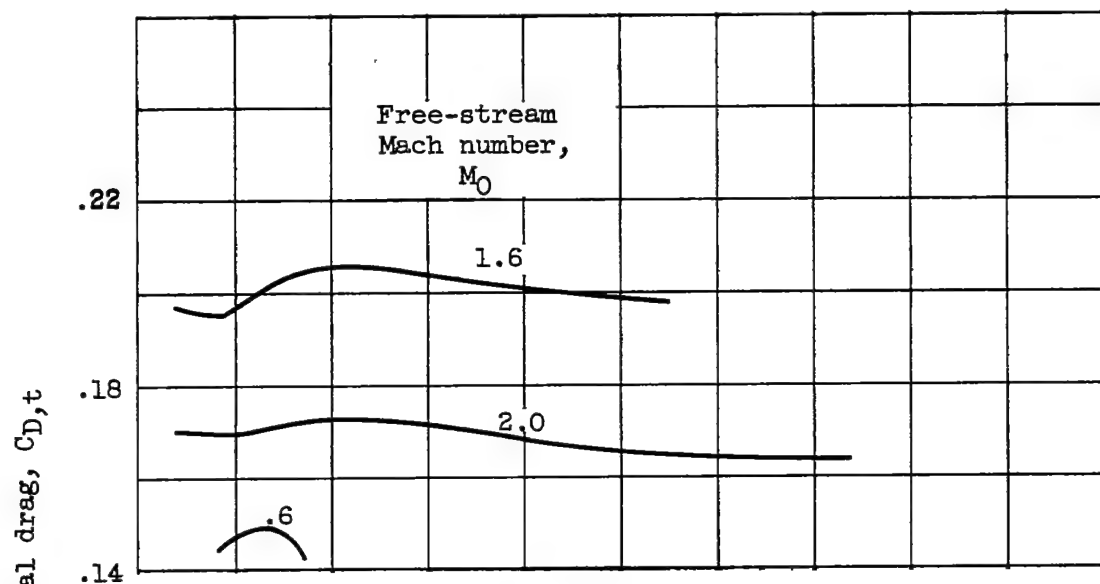
(a) Convergent-divergent plug position.
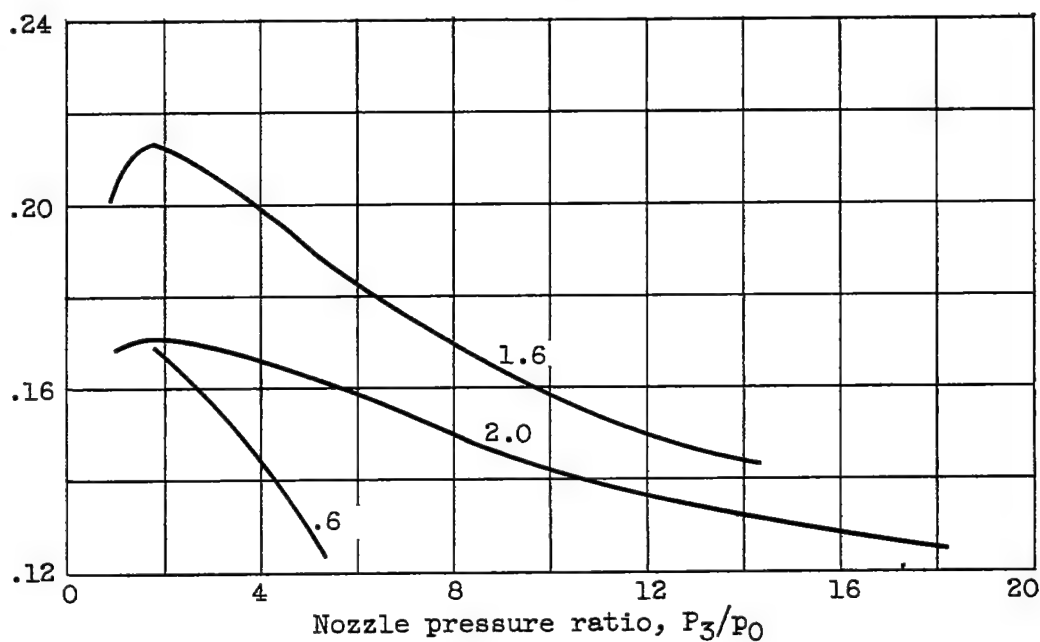
(b) Convergent plug position.

Figure 10. - Variation of total external drag coefficient
with nozzle pressure ratio at zero angle of attack.
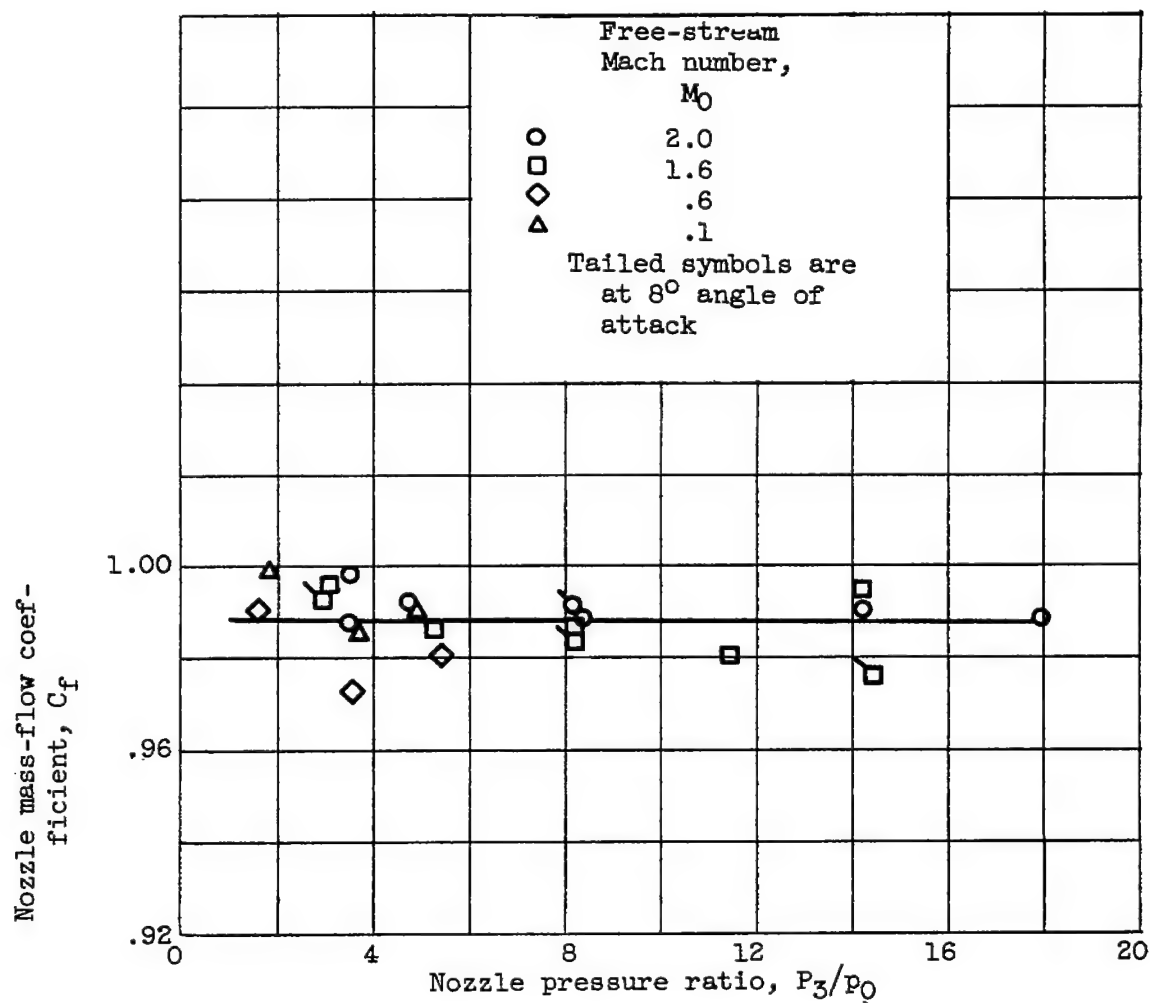
Figure 11. - Variation of nozzle mass-flow coefficient with nozzle pressure ratio for convergent plug position at zero angle of attack.

(a) Convergent-divergent plug position.

(b) Convergent plug position.
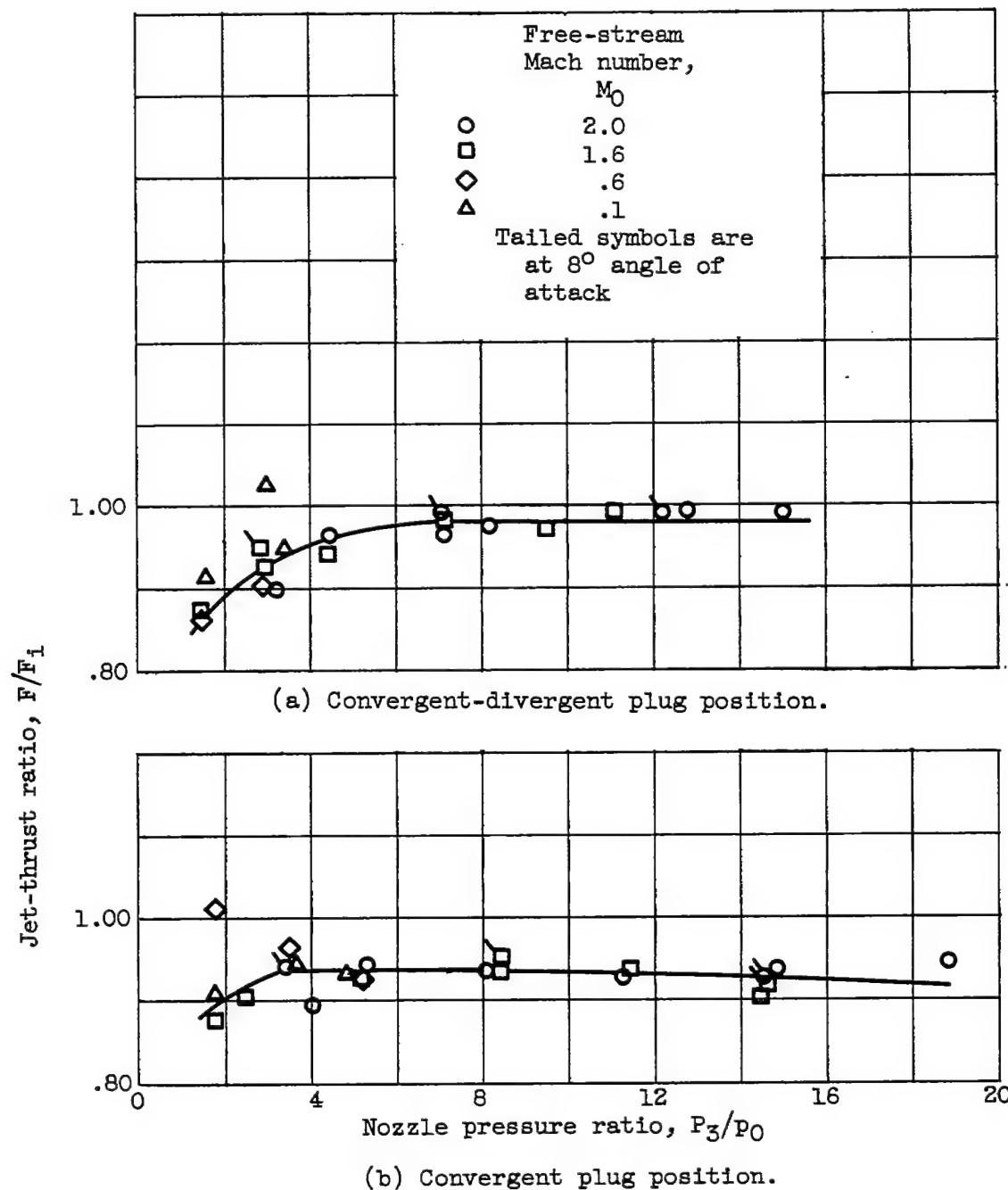
Figure 12. - Variation of jet-thrust ratio obtained from force measurements with nozzle pressure ratio at zero angle of attack.
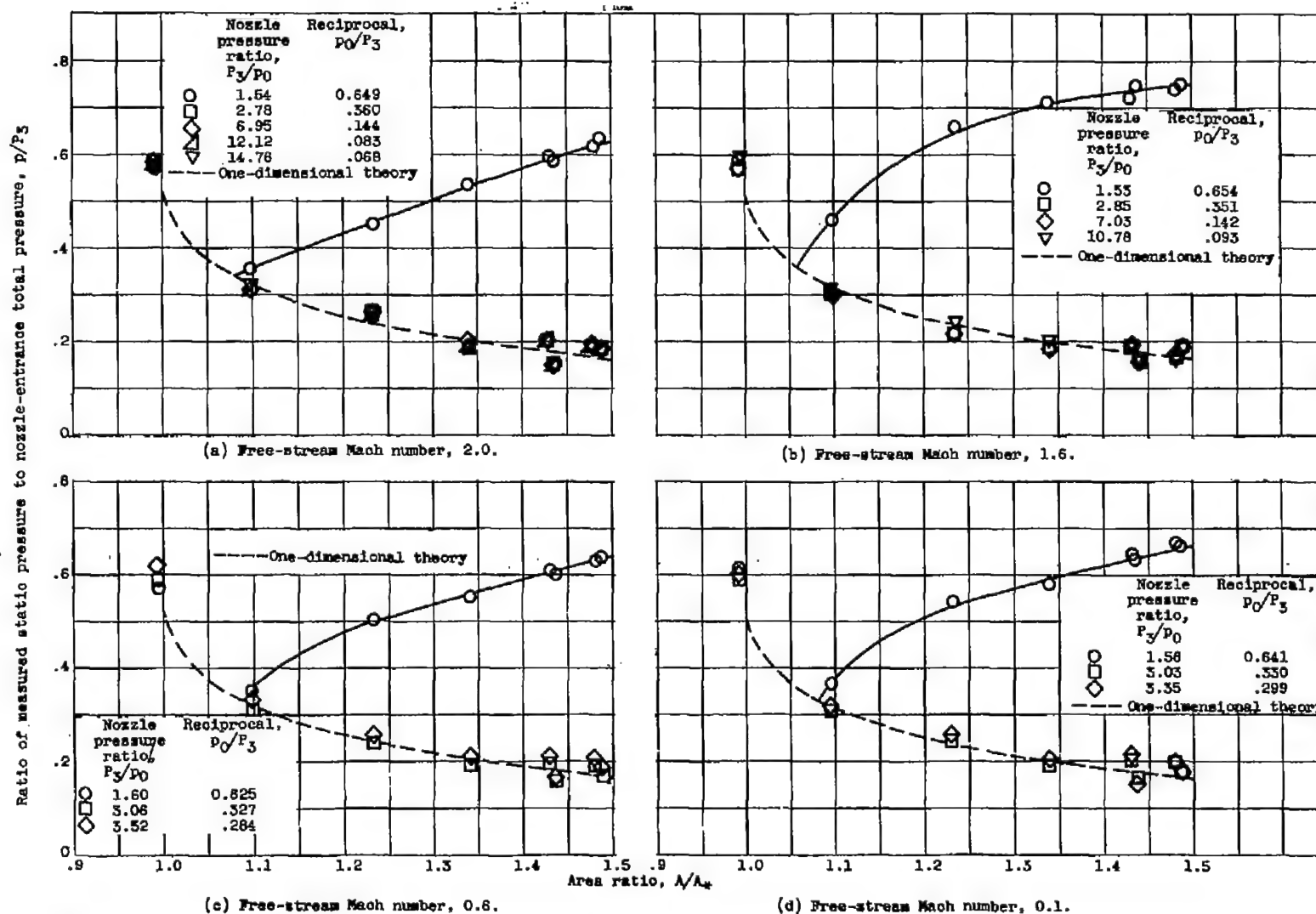
Figure 13. - Static-pressure distribution through diverging section for convergent-divergent plug position at zero angle of attack.
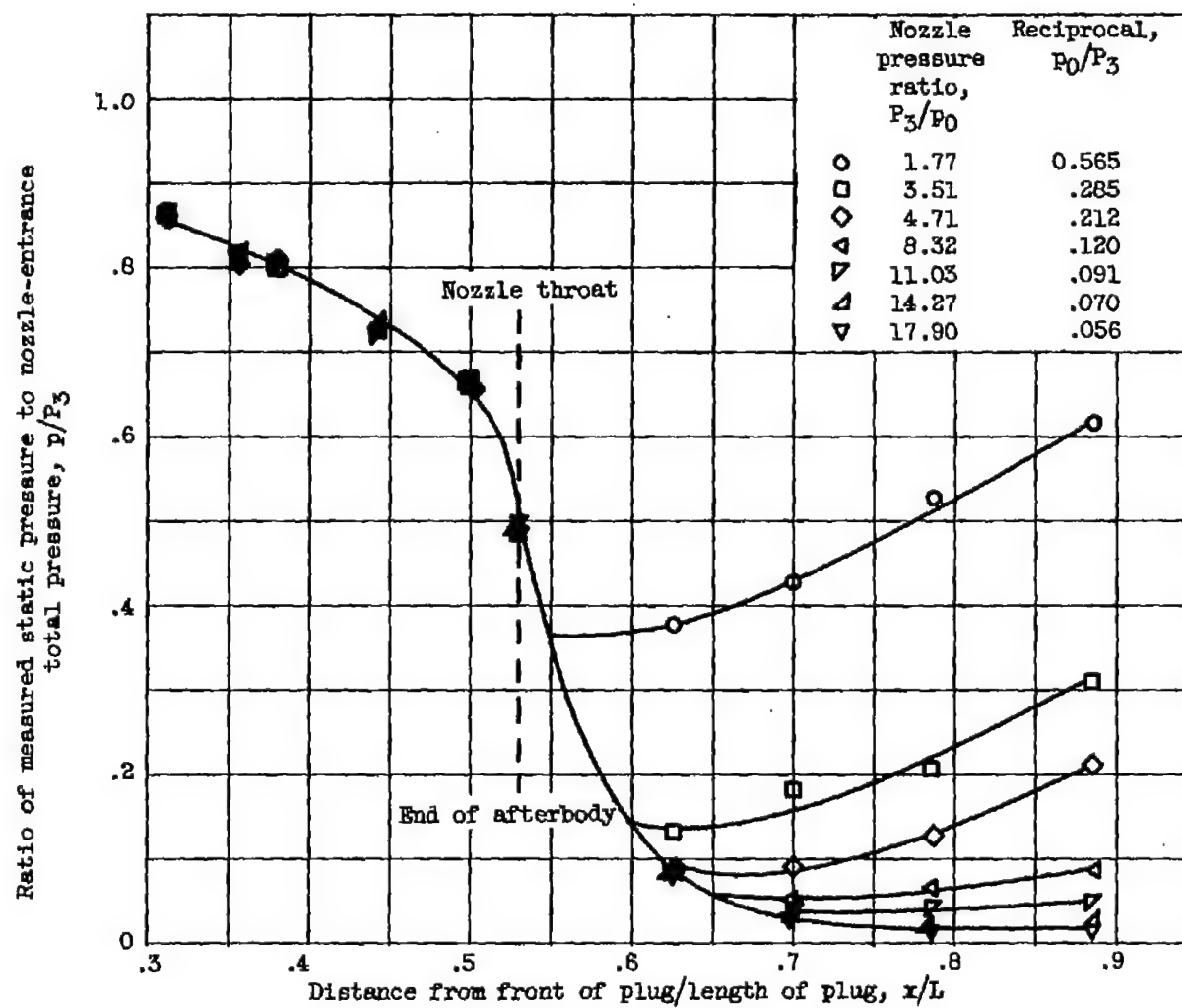
(a) Free-stream Mach number, 2.0.

Figure 14. - Static-pressure distributions along center plug for convergent plug position at zero angle of attack.
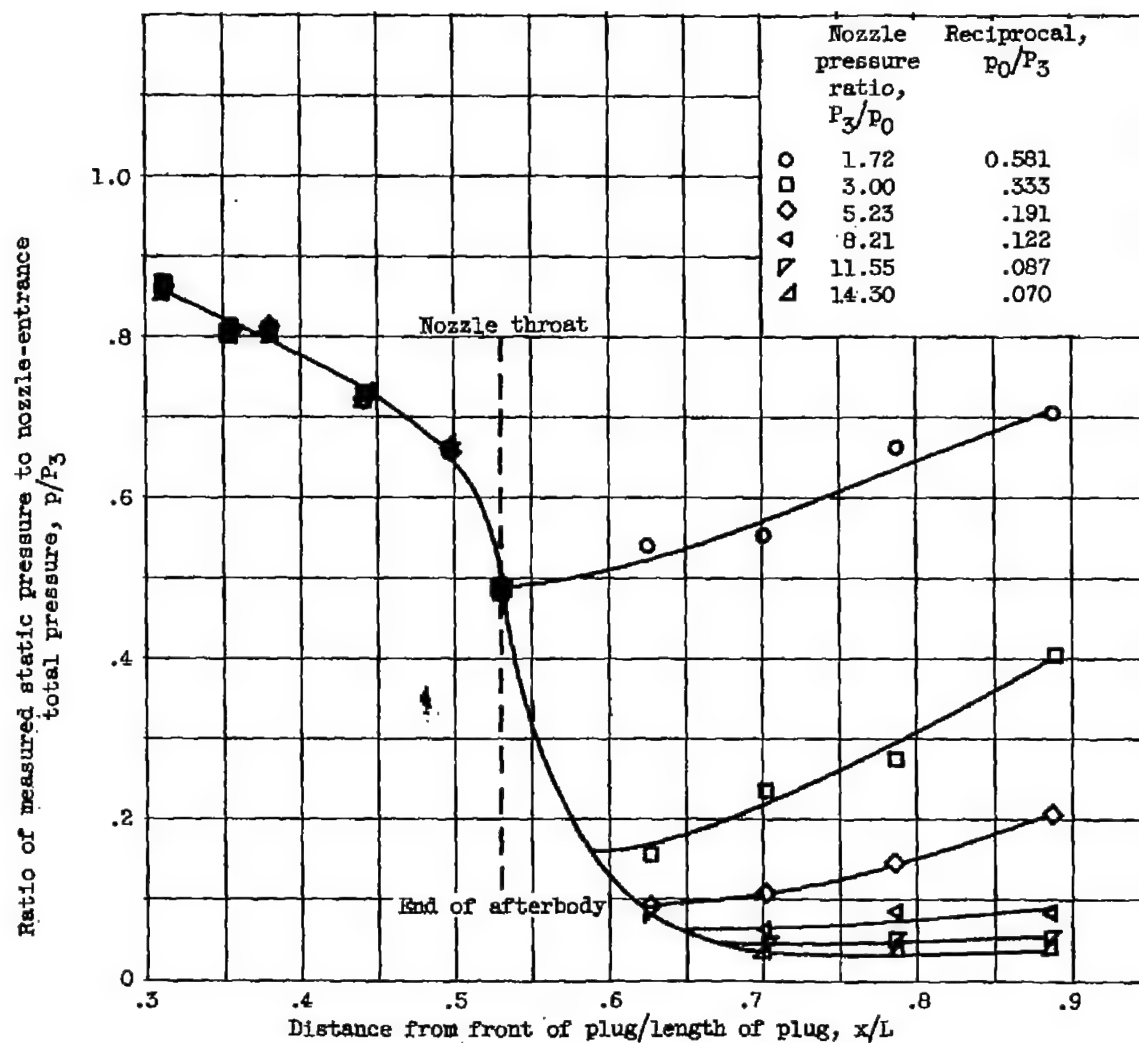
(b) Free-stream Mach number, 1.6.

Figure 14. - Continued. Static-pressure distributions along center plug
for convergent plug position at zero angle of attack.
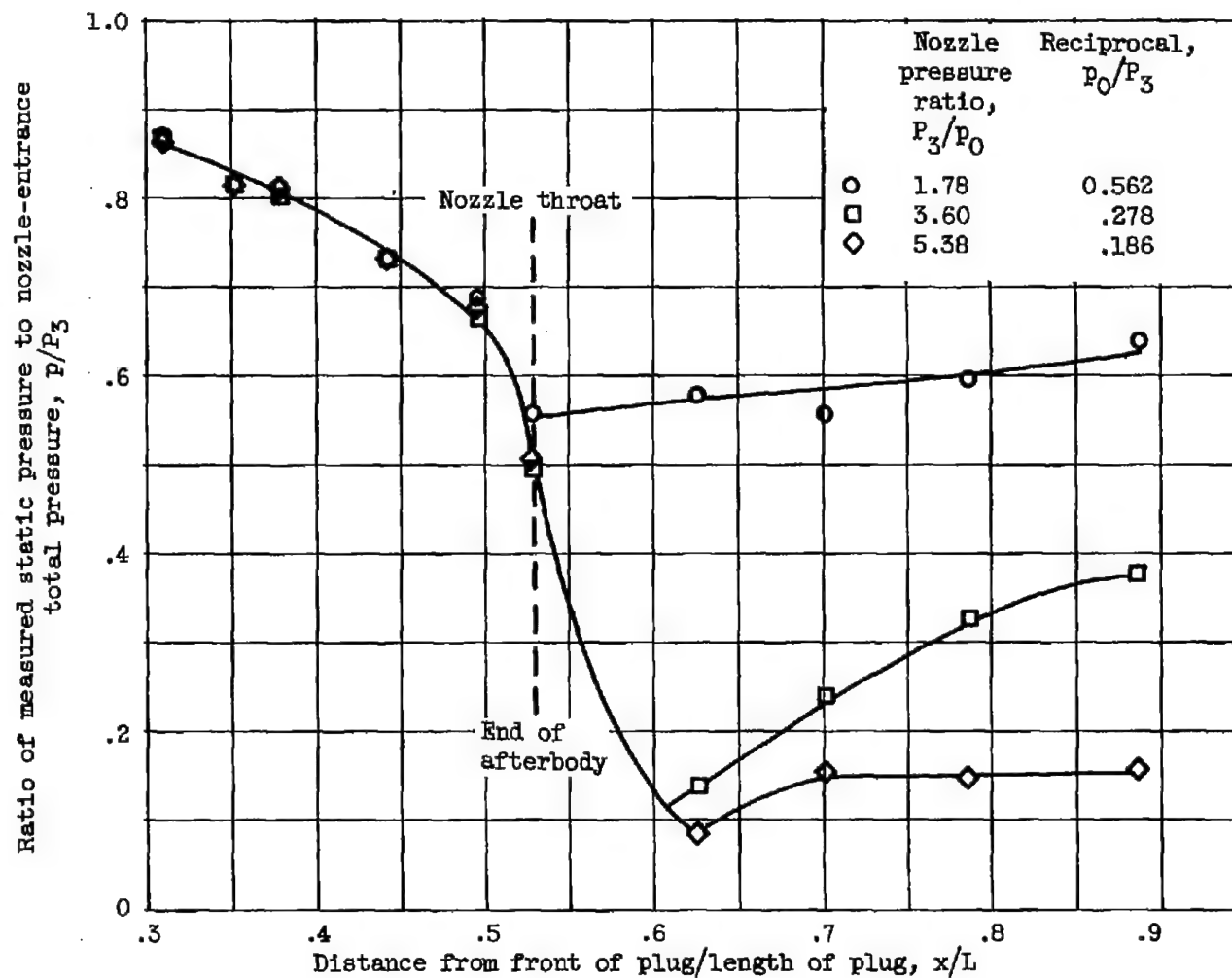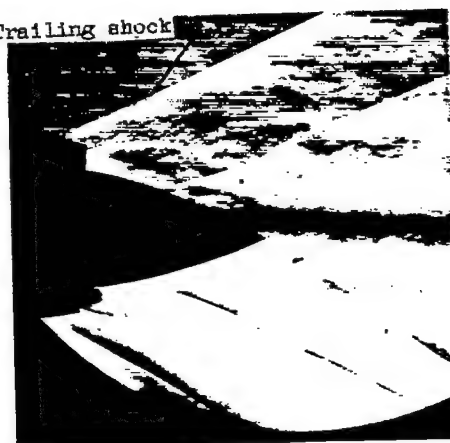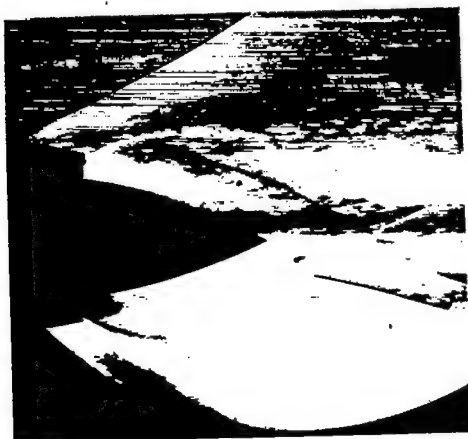
(c) Free-stream Mach number, 0.6.

Figure 14. - Continued. Static-pressure distributions along center plug
for convergent plug position at zero angle of attack.

	Nozzle pressure ratio, P_3/p_0	Reciprocal, p_0/P_3
○	1.85	0.541
□	3.56	.281
◇	4.83	.207
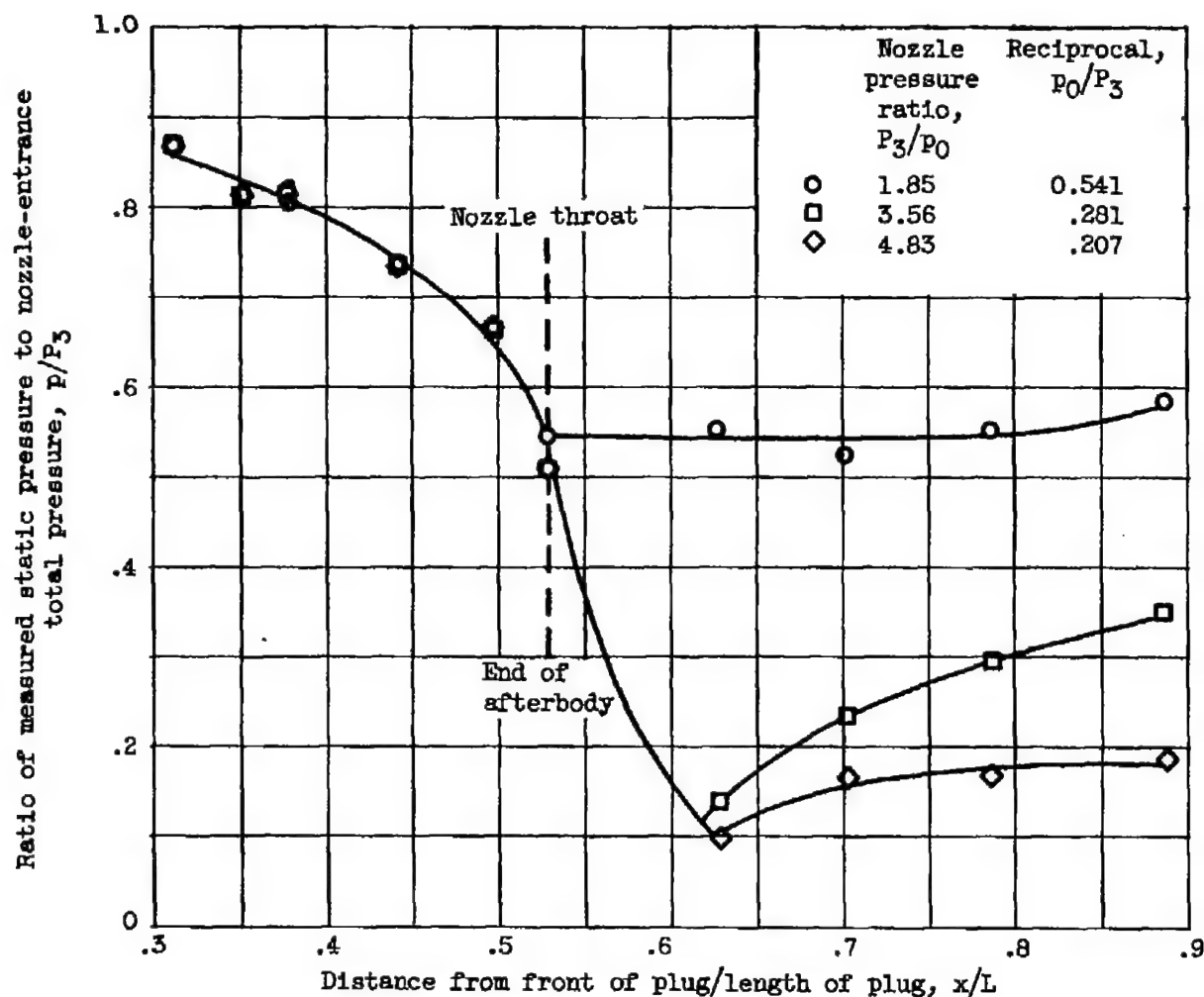
(d) Free-stream Mach number, 0.1.

Figure 14. - Concluded. Static-pressure distributions along center plug for convergent plug position at zero angle of attack.
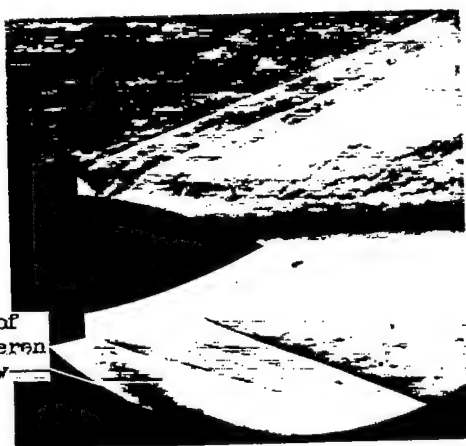
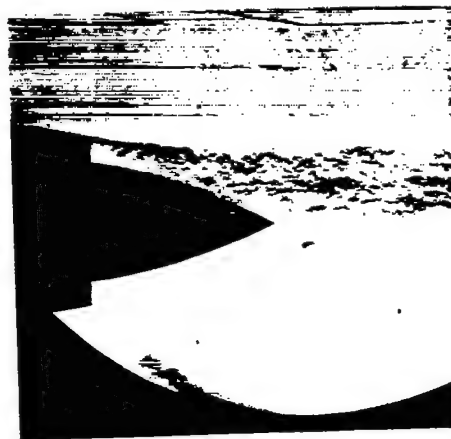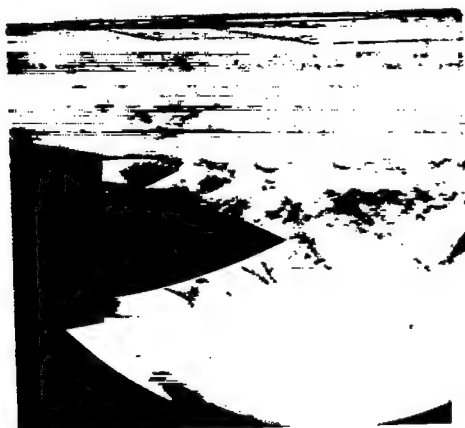(a) Free-stream Mach number, 2.0; nozzle pressure ratio, 1.78.

(b) Free-stream Mach number, 2.0; nozzle pressure ratio, 8.32.

(c) Free-stream Mach number, 2.0; nozzle pressure ratio, 17.90.

(d) Free-stream Mach number, 0.6; nozzle pressure ratio, 1.78.

(e) Free-stream Mach number, 0.6; nozzle pressure ratio, 3.59.

(f) Free-stream Mach number, 0.6; nozzle pressure ratio, 5.39.

Figure 15. - Schlieren photographs of exhaust jet for convergent plug position at free-stream Mach numbers of 2.0 and 0.6 and zero angle of attack.
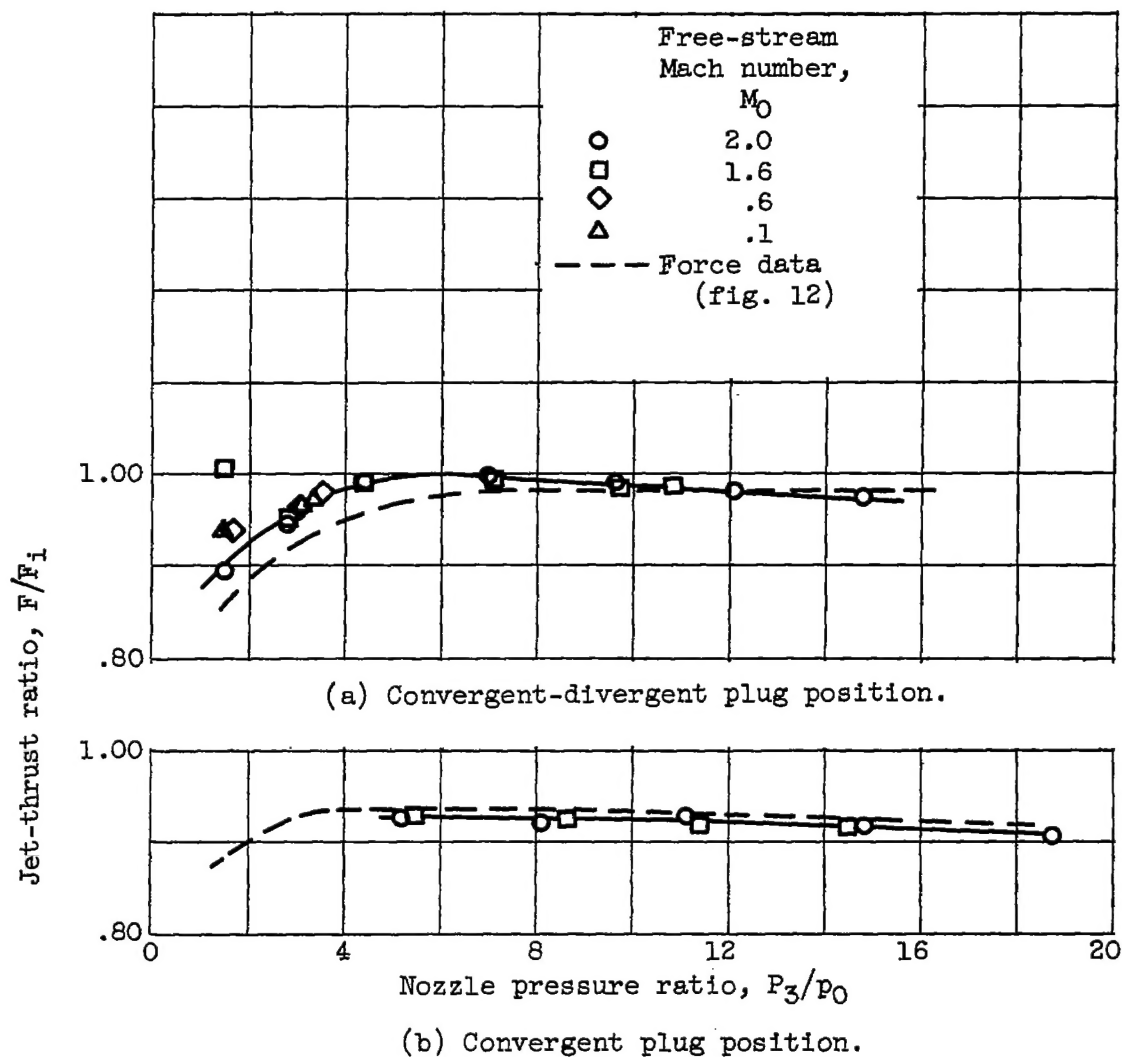
NACA RM E53L16

Figure 16. - Variation of jet-thrust ratio as obtained from pressure integration with nozzle pressure ratio.

(a) Convergent-divergent plug position.

(b) Convergent plug position.

NACA RM E53L16

Free-stream
Mach number,
M_0

○   2.0
□   1.6
◇   .6
△   .1
— — — Force data
(fig. 12)

1.00

.80

Jet-thrust ratio, F/F_i

(a) Convergent-divergent plug position.

1.00

.80

0   4   8   12   16   20

Nozzle pressure ratio, P_3/p_0

(b) Convergent plug position.

Figure 16. - Variation of jet-thrust ratio as obtained from pressure integration with nozzle pressure ratio.

3138

(a) Convergent-divergent plug position.
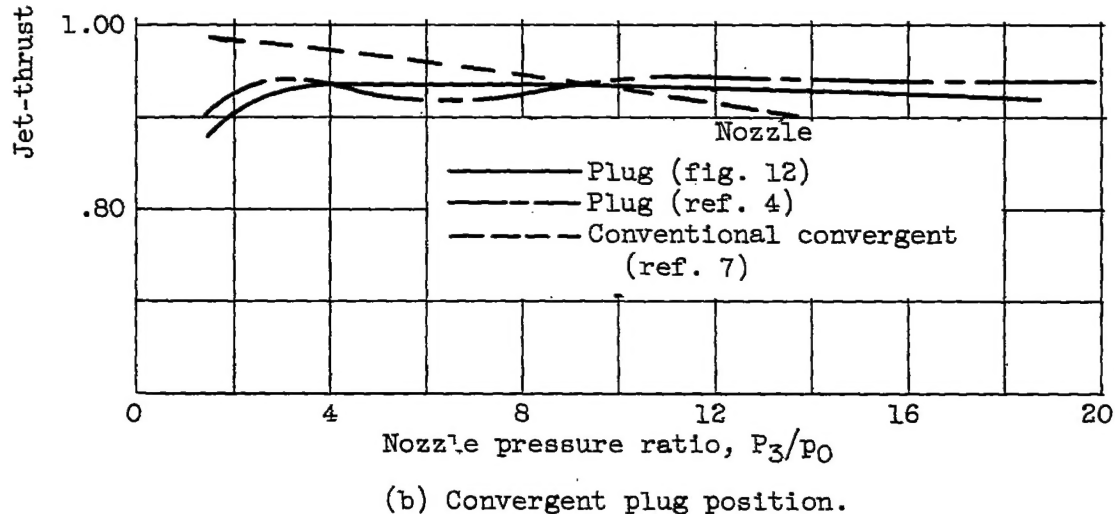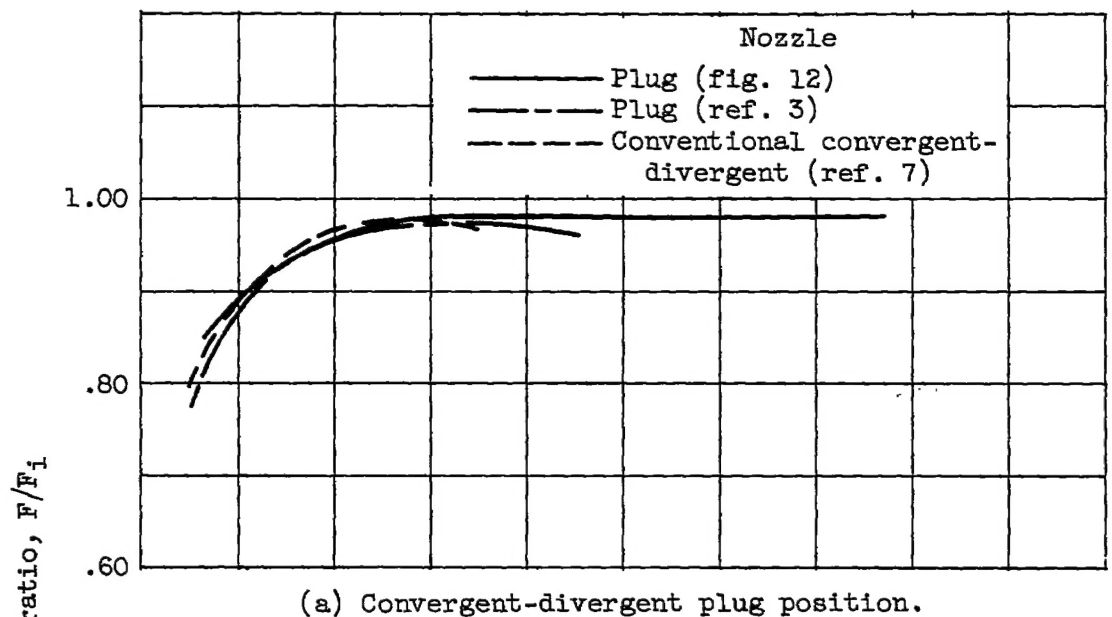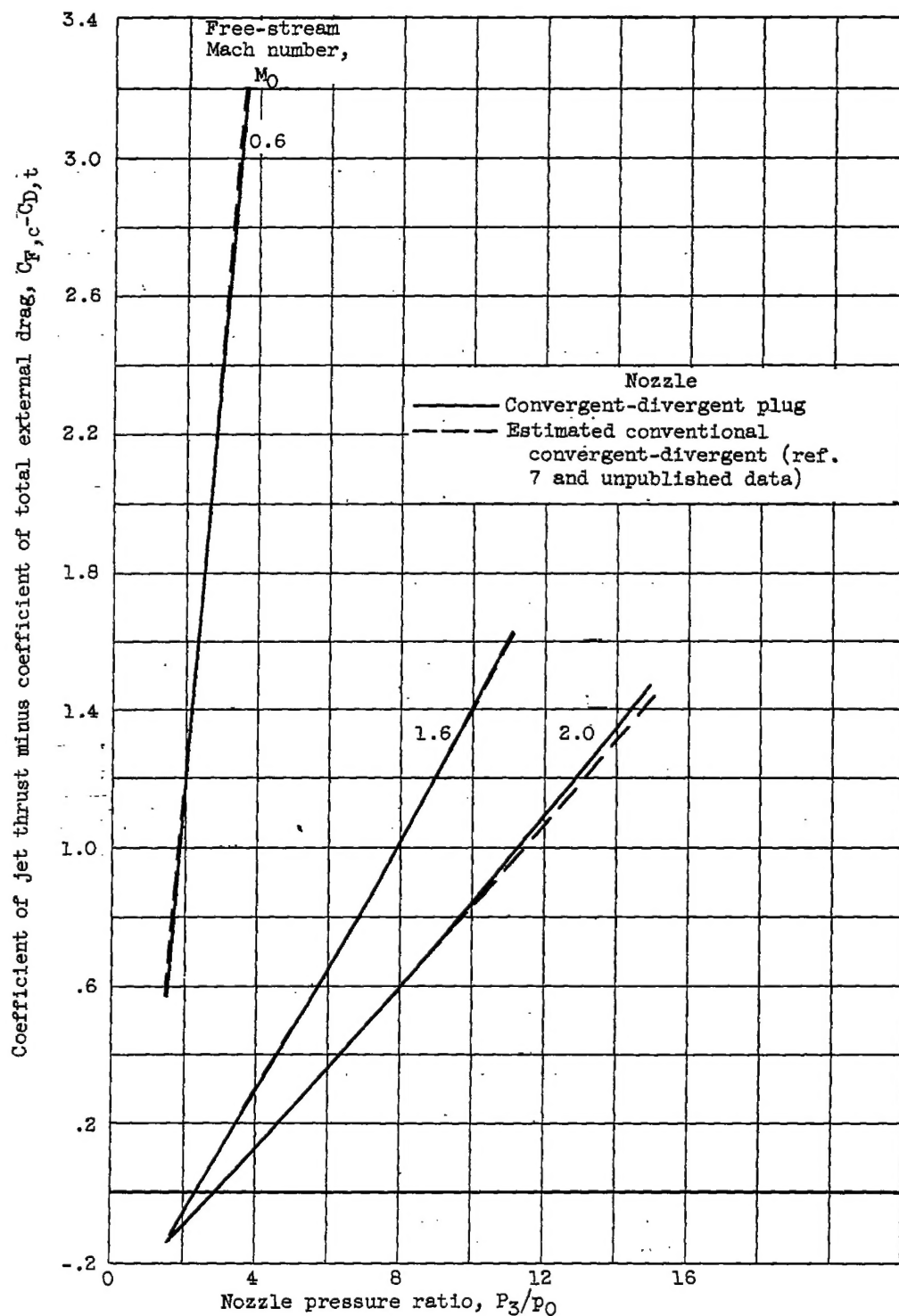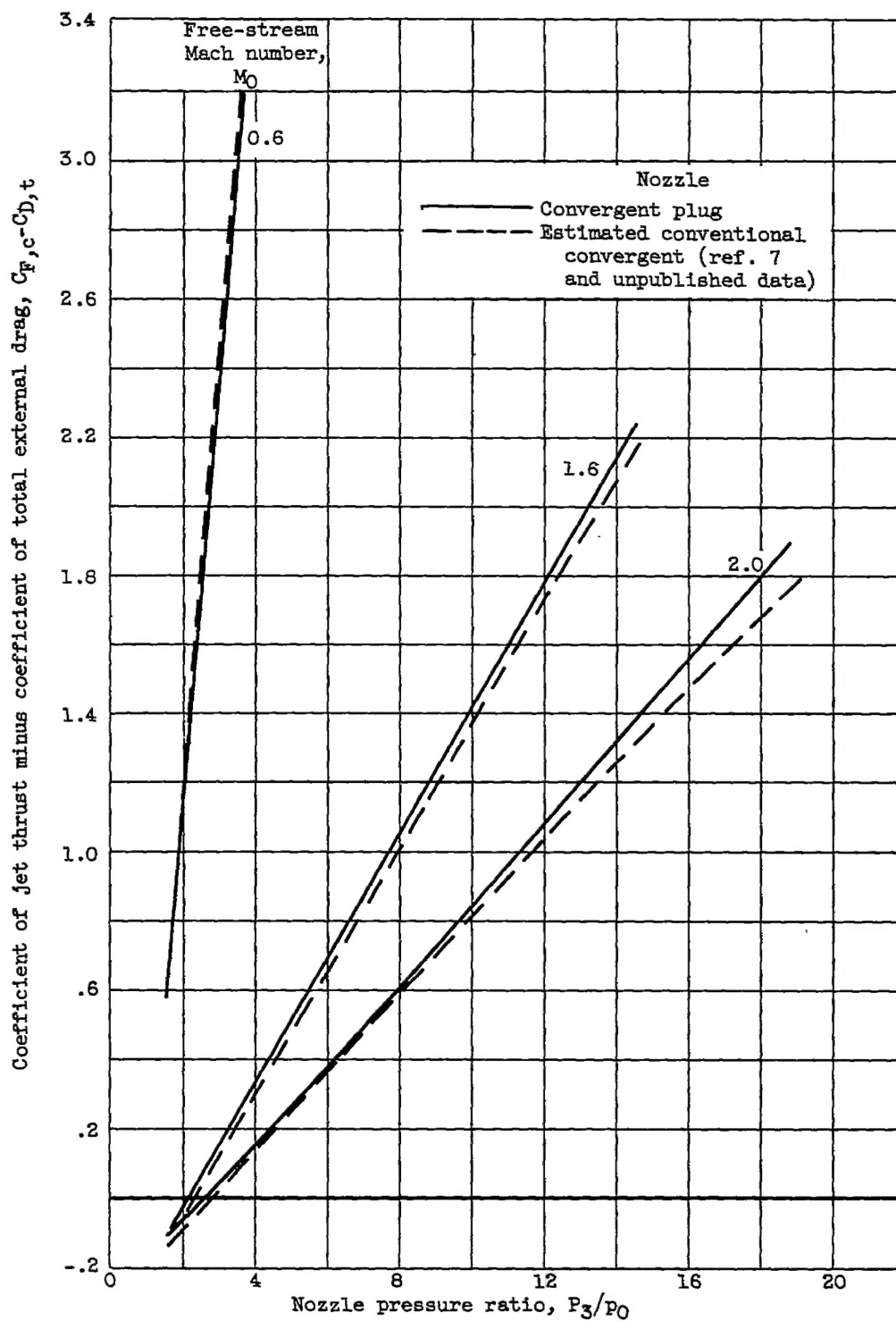
(b) Convergent plug position.

Figure 17. - Jet-thrust-ratio comparison with comparable plug
and conventional-type nozzles investigated in quiescent air.

(a) Convergent-divergent plug position.

Figure 18. - Jet-thrust-minus-external-drag comparison.

3138

(b) Convergent plug position.

Figure 18. - Concluded. Jet-thrust-minus-external-drag comparison.